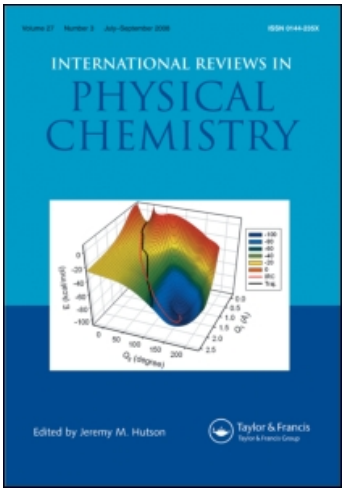

International Reviews in Physical Chemistry
Publication details, including instructions for authors and subscription information:
http://www.informaworld.com/smpp/title~content=t713724383

Laser photoelectron spectroscopy of H_2 and D_2: Competing decay channels in 'simple' molecules

C. A. De Lange[a]
[a] Laboratory for Physical Chemistry, University of Amsterdam, Amsterdam, The Netherlands

Online publication date: 26 November 2010

To cite this Article De Lange, C. A.(2001) 'Laser photoelectron spectroscopy of H_2 and D_2: Competing decay channels in 'simple' molecules', International Reviews in Physical Chemistry, 20: 1, 1 — 32
To link to this Article: DOI: 10.1080/01442350010005131
URL: http://dx.doi.org/10.1080/01442350010005131

INT. REVIEWS IN PHYSICAL CHEMISTRY, 2001, VOL. 20, NO. 1, 1–32

Laser photoelectron spectroscopy of H_2 and D_2: competing decay channels in 'simple' molecules

C. A. DE LANGE†

Laboratory for Physical Chemistry, University of Amsterdam, Nieuwe Achtergracht 127–129, 1018 WS, Amsterdam, The Netherlands

The mechanisms underlying dissociative recombination of H_2^+, D_2^+ and HD^+ have been a matter of considerable debate. Superexcited states belonging to two different categories, leading to the so-called direct and indirect processes, are usually considered. The direct process involves doubly excited repulsive Rydberg states, which, at lower energies, possess configurations $(2p\sigma_u)(nl\lambda)$, forming Rydberg series converging upon the $^2\Sigma_u^+(2p\sigma_u)$ ionic limit, or, at higher energies, have configurations $(2p\pi_u)(nl\lambda)$, leading to series converging upon the $^2\Pi_u(2p\pi_u)$ ionic state. In the indirect process, vibrationally excited levels of singly excited bound Rydberg states with configurations $(1s\sigma_g)(nl\lambda)$, which form Rydberg series converging upon the $X\ ^2\Sigma_g^+(1s\sigma_g)$ ionic threshold, are thought to play a key role. Experimental studies of dissociative recombination are fraught with difficulties. In this contribution we shall explore the uses and advantages of resonance-enhanced multiphoton ionization, either with kinetic-energy-resolved electron detection (termed laser photoelectron spectroscopy), or with mass-resolved ion detection, to investigate the role of these superexcited states. Experiments via the $B\ ^1\Sigma_u^+$ intermediate state were carried out on H_2 and D_2 with (3+1) one-colour laser photoelectron spectroscopy, and on H_2 with a (1+1′) two-colour scheme employing ion detection. In our experiments, competition between direct molecular ionization, autoionization and (pre)dissociation was apparent. Above the dissociation threshold at which atoms in the ground and $n = 3$ excited states are formed, the formation of molecular ions and of excited $n = 2$ fragments was virtually terminated, to be replaced by the generation of $n = 3$ fragments. Our observations can be explained by invoking a mechanism, which so far has not received much attention, namely the direct excitation of vibrational continua of singly excited Rydberg states.

Contents

† Email: delange@fys.chem.uva.nl

International Reviews in Physical Chemistry ISSN 0144-235X print/ISSN 1366-591X online © 2001 Taylor & Francis Ltd
http://www.tandf.co.uk/journals
DOI: 10.1080/01442350010005131

1. Introduction

Dissociative recombination (DR) describes the process in which a monopositive molecular ion captures an electron into a highly excited state of the neutral molecule, followed by dissociation into neutral atomic or molecular fragments:

$$AB^+ + e^- \rightarrow AB^* \rightarrow A + B.$$

The dissociation process is in competition with autoionization of the highly excited state AB* in which the electron is re-emitted and the original molecular ion is formed again. The DR process is particularly significant in removing molecular ions from astrophysical plasmas. A detailed knowledge of the cross-sections and branching ratios into neutral fragments is important in order to understand the physics and chemistry of these plasmas. Clearly research on the DR of the simplest molecular ion, H_2^+, and its isotopomers D_2^+ and HD^+, has been crucial in obtaining an understanding of the fundamental issues that play a role. Despite the apparent simplicity of molecular hydrogen and its isotopomers, and notwithstanding large experimental and theoretical efforts by several research groups, many aspects that have to do with the dynamics of the dissociation process and the branching into neutral ground state and excited-state atomic fragments are still not completely understood. In fact, the often suggested 'simplicity' of the hydrogens is in many ways deceptive because, despite extensive experimental and theoretical research carried out on these molecules during the last 70 years, many characteristics of excited states in general remain unexplained.

Experimentally there is a serious problem in producing the parent ions for the DR process in their vibrational ground state only. In particular, for the homonuclear diatomic species H_2^+ and D_2^+, which lack an electric dipole moment, radiative vibrational relaxation is forbidden and therefore very slow. Since the DR cross-section rises steeply as a function of the vibrational quantum number, it is in practice not easy to extract results for the vibrational ground state alone. The situation is somewhat better for HD^+ which undergoes faster radiative vibrational deactivation. Experimental techniques which have been employed consist of flowing afterglow techniques [1, 2], the use of inclined beams [3], hollow electron-beam traps [4] and merged-beam methods [5–7]. More recently, the use of ion storage rings in conjunction with electron-cooler technology has been employed with some success. With the latter technique, electron energies have to be controlled very accurately, and only recently have storage ring experiments developed to the point where this is feasible [8]. Applications to the DR of molecular hydrogen and its isotopomers have now been performed [9–14], and (absolute) cross-sections [9, 10, 12, 13] and product state information [11, 13, 14] have

been obtained. However, since the product state resolution inherent in these storage ring experiments is limited, a complete description of the dissociation process still remains difficult.

A complete theoretical description of DR provides its own challenges. The DR process can be viewed as consisting of three parts:

(i) the electron capture process;
(ii) the ensuing competition between autoionization which returns the situation to its starting point, and dissociation;
(iii) for excited molecules which 'survive' autoionization, the actual molecular dissociation takes place, which can be viewed as a half collision process.

The DR cross-section is determined by (i) and (ii), the dynamics, final product distributions and angular distributions following dissociation by (iii).

The question of which highly excited molecular states play a key role in the electron capture process in H_2^+, D_2^+ and HD^+ had been a matter of considerable debate. Bates [15] was the first to emphasize the importance of doubly excited repulsive Rydberg states converging upon the $^2\Sigma_u^+$ $(2p\sigma_u)$ ionic state. In particular, the lowest of these states, $^1\Sigma_g^+$ $(2p\sigma_u)^2$, is important at energies not too far above the ionization threshold (less than 3 eV) of molecular hydrogen. This mechanism, which involves doubly excited Rydberg states with configurations $(2p\sigma_u)(nl\lambda)$, is known as the direct process. At higher energies a second group of dissociative Rydberg states with configurations $(2p\pi_u)(nl\lambda)$, belonging to series converging upon the $^2\Pi_u(2p\pi_u)$ ionic state, participates as well. Later Bardsley [16] introduced the notion of indirect processes, in which vibrationally excited Rydberg states with configurations $(1s\sigma_g)(nl\lambda)$, belonging to singly excited Rydberg series converging upon the X $^2\Sigma_g^+(1s\sigma_g)$ ionic core, should be considered. An additional complication has been pointed out by Chupka [17] in a discussion of multiphoton ionization and subsequent dissociation of H_2. The dissociation process is strongly affected by a large series of interactions between doubly excited repulsive Rydberg states and singly excited bound molecular Rydberg states of the same symmetry at large internuclear separations. A multitude of outgoing channels has to be addressed, leading to a final state distribution which is difficult to predict. For a complete description the interaction strengths at every avoided crossing should be known. For an adequate description a full multichannel treatment based on such couplings is required [14]. Other theoretical treatments consist of the extension of the configuration interaction method [18], and the application of multichannel quantum defect theory [19, 20] with the inclusion of dissociative channels [12, 18, 21].

The presence and interplay of doubly excited Rydberg states and of excited vibrational levels of singly excited Rydberg states of the neutral molecule are clearly essential in any predictive theoretical treatment of DR. All these states are located (at internuclear distances close to the equilibrium distance of the molecular ground state) *above* the lowest ionic threshold of the molecule and are termed superexcited states. Independent experimental information on such superexcited states cannot in general be obtained easily. In this contribution we shall explore the uses and advantages of resonance-enhanced multiphoton ionization (REMPI) spectroscopy, often with kinetic-energy-resolved electron detection (i.e. photoelectron spectroscopy (PES)), for the study of superexcited states in molecular hydrogen and its isotopomers in some detail. REMPI–PES is often termed laser photoelectron spectroscopy for short.

With the availability of lasers with high pulse energies in the visible and ultraviolet (UV) portion of the spectrum, the experimentalist can now go beyond the realm of

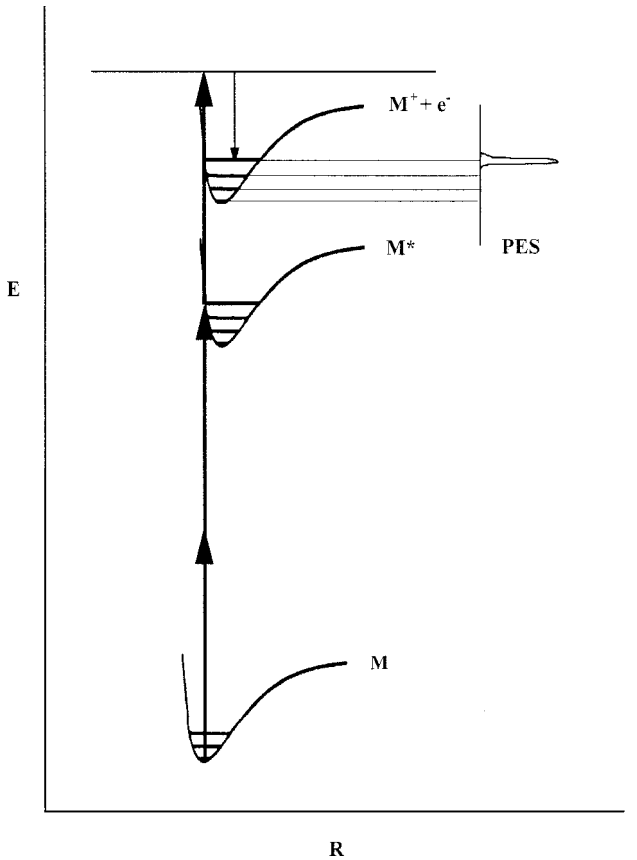

Figure 1. Schematic diagram of a (2+1) REMPI process.

one-photon methods and utilize processes involving the absorption of more than one photon. The optical selection rules associated with multiphoton absorption are strict but do depend on the number of absorbed photons. This provides for a degree of flexibility, which removes many of the limitations which plague one-photon absorption spectroscopy, in that a much wider range of molecular excited states can be accessed. Another feature to be stressed is the fact that with the absorption of one or more additional photons the ionization threshold of the molecule can be exceeded and that essentially every molecule can thus be photoionized. This ionization step is again subject to selection rules, but these do not form a serious constraint on the final state reached, since the outgoing electron can take away the required excess energy and angular momentum. A schematic diagram of a (2+1) REMPI process is presented in figure 1. Because the excited states are mapped efficiently and with few restrictions on to an ionic state, which is often well known, the REMPI method is very general and highly suitable for the detailed observation of such states. The occurrence of the ionization process can be monitored either by relatively simple mass-resolved ion detection [22, 23], or by experimentally much more demanding kinetic-energy-resolved photoelectron detection (i.e. PES) [24–29]. With the latter method, considerations of energy and momentum conservation allow the experimentalist to determine the internal energies of the ions formed in the two-step process. The determination of ion internal energies (electronic, vibrational and rotational) is a true asset of the method,

and laser photoelectron spectroscopy offers very significant advantages for the study of molecular excited states which are not easily matched in its broad applicability by other techniques.

When considering multiphoton absorption in a molecule, a variety of processes can occur. Of course, depending on the total photon energy deposited into the molecule, one or more molecular ionization continua can be addressed and direct molecular ionization occurs. However, in a significant number of cases a competing process involving multiphoton absorption to a neutral superexcited state takes place. Since superexcited states are by definition metastable, they can undergo a variety of decay processes, which usually lead to short lifetimes. The direct observation of superexcited states is therefore not very common [30–33]. However, despite the fact that the role of superexcited states is usually only indirect, their significance in laser photoelectron spectroscopy can hardly be overestimated [32, 34–38]. Their decay channels include autoionization, in which an electron is lost into lower-lying ionization continua, or molecular (pre)dissociation into smaller neutral fragments, in either their ground or their excited states. Fragments formed in sufficiently high excited states can be subsequently photoionized in the strong photon field required to induce the multiphoton process in the first place. The unique power of laser photoelectron spectroscopy lies in the fact that all these competitive decay channels can be observed and compared quantitatively at the same time [32, 38].

The method of laser photoelectron spectroscopy is highly sensitive when appropriate experimental procedures are employed. In our group in Amsterdam we rely heavily on the use of a 'magnetic bottle' analyser which was developed into a very flexible tool for high-resolution kinetic-energy-resolved electron detection [39–42]. With the available techniques the resolution in the photoelectron spectra is usually sufficient to resolve molecular electronic and vibrational levels, while in favourable cases, such as the molecular hydrogens and other diatomic hydrides, separate rotational levels in the ion can be observed as well. When this is the case, the essential role of angular momentum in the photoionization process and the associated photoionization dynamics can be studied experimentally.

In order to obtain independent information about which superexcited states in the hydrogens play a role in dissociation processes, we can access an intermediate excited state in a multiphoton absorption scheme from below and study the subsequent dissociation dynamics after absorption of one or more additional photons. The molecular dissociation process is formally independent from the way in which dissociative states are formed. Of course a multiphoton study requires a suitable intermediate excited state as a stepping stone. Multiphoton absorption studies of molecular hydrogen via B $^1\Sigma_u^+$ [43–47], C $^1\Pi_u$ [45, 48–51], EF $^1\Sigma_g^+$ [52–60], B′ $^1\Sigma_u^+$ [59–61], B″ $^1\Sigma_u^+$ [59] and D $^1\Pi_u$ [59, 61] have been utilized for that purpose. Research of this type has amply demonstrated the importance of doubly excited repulsive states on the photoionization and photodissociation dynamics. In our experiments to be described in the present contribution we shall study the photoionization and dissociation dynamics of molecular hydrogen and deuterium via excitation of the B $^1\Sigma_u^+$ $(1s\sigma_g)(2p\sigma_u)(v'; N')$ state from the X $^1\Sigma_g^+$ $(1s\sigma_g)^2$ ground state. This transition is allowed with an odd number of photons. From the B $^1\Sigma_u^+$ state a variety of subsequent one-photon processes can be envisaged. First, the molecule can directly ionize into the ionization continua of the ground ionic state X $^2\Sigma_g^+$ $(1s\sigma_g)$. Secondly, doubly excited states with configuration $(2p\sigma_u)(nl\lambda)$ can be excited. These states may either autoionize into the continua of the ionic ground state or undergo

dissociation, resulting in a ground-state (1s) atom and an excited ($n'l$) atom (where n' may differ from n). Thirdly, a possibility which until now has received little attention is that singly excited Rydberg states of configuration $(1s\sigma_g)(n''l\lambda)$, and in particular their dissociative continua, may be assessed.

In our experiments on H_2 and D_2, both molecular ionization and dissociation into a ground-state fragment and an excited atom ($n \geqslant 2$) are observed at the same time. Laser photoelectron spectroscopy offers a distinct advantage in that the final states reached in the dissociation process can be monitored reliably through one-photon ionization of excited hydrogen atoms. With our photon energies employed, all hydrogen atoms with $n \geqslant 2$ can be ionized. With our resolution of about 10 meV, electrons ejected from excited atoms with principal quantum numbers from $n = 2$ to $n = 8$ can be resolved, while signals arising from atoms with higher n merge. The same technique allows us to determine the internal energies of the molecular ions formed in the direct ionization process with rotational resolution. In the following we shall describe (3+1) REMPI–PES on H_2 [35] and D_2 [37] and, additionally, (1+1′) REMPI experiments on H_2 [36] via the $B\ ^1\Sigma_u^+$ intermediate state. In general, our work on the hydrogens provides a convincing example of the crucial role played by superexcited states in multiphoton absorption processes. More specifically, our experiments will emphasize the role of dissociative continua of singly excited Rydberg states belonging to series converging upon the $X\ ^2\Sigma_g^+$ ionic ground state in the photoionization and photodissociation dynamics of the $B\ ^1\Sigma_u^+$ state [35–37].

2. Experimental details

2.1. (3+1) resonance enhanced multiphoton ionization–photoelectron spectroscopy experiments on H_2 and D_2 via $B\ ^1\Sigma_u^+$

Our laser photoelectron spectroscopy experiments on H_2 and D_2 at the University of Amsterdam discussed in the present contribution are carried out with a time-of-flight (TOF) 'magnetic bottle' electron analyser, equipped with an effusive beam sample inlet system. This spectrometer is based on the original design of Kruit and Read [39] in which the multiphoton ionization process takes place in the focused beam of a pulsed laser with a high photon flux. The focus is situated in the high-field portion of an inhomogeneous magnetic field, which decreases from 1 T in the focus to 10^{-3} T in the flight tube 50 cm long. The trajectories of the ejected electrons with a velocity component in the direction of the flight tube are made parallel in such a way that electrons ejected with the same kinetic energy arrive at virtually the same time at the microchannel plates which are used as detectors at the end of the flight tube. Under appropriate experimental conditions the collection efficiency approaches 50% and for this reason the term '2π analyser' is often used. The parallelization process takes place in the first few millimetres of the electron flight path, a small distance compared with the total length of the flight tube. Two pole faces to which insulated grids are attached for accelerating and decelerating voltages supply the magnetic field in the focal region. Furthermore, electrons can be retarded in the flight tube, after their trajectories have been made parallel. Employing two pairs of mutually perpendicular Helmholtz coils compensates the Earth's magnetic field in the ionization region and the flight tube. Using judiciously chosen retarding voltages a typical resolution for the electron's kinetic energy of about 10 meV can be achieved for appreciable periods of time, even under experimental conditions involving the presence of reactive short-lived species which may react with critical surfaces of the spectrometer [40, 41]. In addition, this type of analyser can be easily adapted to mass-resolved TOF ion detection, and, when

better resolution is required to zero-kinetic-energy electron detection with essentially laser-limited resolution [62]. For a much more detailed description of the spectrometer the reader is referred to a recent paper by Rijs *et al.* [42].

The laser system employed in conjunction with the 'magnetic bottle' spectrometer consists of a XeCl excimer laser (Lumonics HyperEx-460) operating at a 30 Hz repetition rate and providing typically 170 mJ in a 10 ns pulse. The excimer laser can pump two dye lasers (Lumonics HyerDye-500) with a bandwidth of about 0.08 cm^{-1} operating on various dyes. The dye laser output can be frequency doubled using a Lumonics Hypertrak-1000 unit equipped with a β-barium borate (β-BaB_2O_4, BBO) or potassium dihydrogen phosphate (KH_2PO_4, KDP) nonlinear crystal. The output, which is polarized parallel to the TOF axis of the spectrometer and which again has a width of about 10 ns, is focused into the 'magnetic bottle' spectrometer using a quartz lens with a focal length of 25 mm. In order to avoid space-charge effects, the laser power is kept as low as possible. The polarization of the laser light can be changed from linear to circular by means of a home-made Fresnel rhomb. For calibration of both the wavelengths and the photoelectron kinetic energies, well known resonances of noble gas atoms are usually employed [41, 42].

2.2. (*1+1′*) *resonance-enhanced multiphoton ionization experiments on* H_2 *via* $B\ ^1\Sigma_u^+$

In separate (1+1′) REMPI experiments on H_2, carried out at the Vrije Universiteit in Amsterdam, a single extreme ultraviolet (XUV) photon was used to excite the H_2 molecule from the $X\ ^1\Sigma_g^+$ electronic ground state to selected rovibrational levels of the $B\ ^1\Sigma_u^+$ excited state. A second tuneable photon was scanned continuously across the H(n = 1)+H(n = 3) dissociation limit, to excite the molecule from $B\ ^1\Sigma_u^+$ to this specific energy region above the lowest ionic $X\ ^2\Sigma_g^+$ threshold.

The experimental set-up and the performance of the XUV laser source have been described before [63, 64] and will only be discussed briefly here. The output of a pulsed dye laser (PDL), pumped by the second harmonic of a neodymium-doped yttrium aluminium garnet (Nd:YAG) laser, is frequency doubled in a KDP crystal, resulting in UV radiation with approximately 35 mJ per pulse. Tuneable XUV radiation is produced via frequency tripling by focusing the UV beam into a xenon gas jet. The XUV and UV radiation are separated by means of a spectral filter which consists of a rod (diameter d = 1.5 mm) placed in the intensity centre of the UV beam in front of the lens and a slit at a distance of about 10 cm behind the focus. The rod creates a vertical line shadow in the UV beam, so that the spatial profile of the UV beam behind the focus differs from the XUV profile. A considerable fraction of the XUV is generated in the shadow of the rod and passes through the slit which cuts off the UV. Hence a pure XUV beam is produced propagating in the forward direction.

The laser light for the second step, which is scanned continuously, is obtained from a second Nd:YAG pumped PDL. The photon energy for the second absorption step ranges from 23000 to 23800 cm^{-1}, which is too low for one-photon ionisation of H(n = 2) fragments, but high enough to ionize hydrogen atoms formed with $n \geqslant 3$. The intensity is kept low to avoid multiphoton ionization processes that might give rise to parasitic signals in the detection of n = 3 fragments.

The counterpropagating laser beams perpendicularly cross a pulsed molecular beam seeded with H_2, which enters through a skimmer into the interaction region. The frequency-doubled output of a Nd:YAG laser is used to photoionize H(n = 3) fragments. A delay of 20 ns was used for these 532 nm pulses with respect to the two other laser beams, in order to avoid the influence of the 532 nm beam on molecular

ionization processes. This frequency is again high enough to ionize H(n = 3) with a single photon, but too low to ionize H(n = 2). In this way, the yield of H(n = 3) fragments as a function of the wavelength can be determined simply by detecting H^+ ions. The ions are extracted from the ionization region by a pulsed electric field, which is delayed with respect to the laser pulses. Ions are mass selected in a field-free TOF tube and collected at an electron multiplier. The signal from the electron multiplier is integrated by two boxcar integrators with their timing windows set for H^+ and H_2^+ ions.

Since the rovibronic energy levels of the B $^1\Sigma_u^+$ state are known accurately [65, 66], only the laser light for the second excitation step has to be calibrated. For this purpose, a Te_2 absorption spectrum is recorded simultaneously with the H^+ and H_2^+ spectra. By assigning the peak positions with the Te_2 atlas [67], an accurate frequency scale is constructed.

The gases were purchased commercially, H_2 (purity 99.9995%) was obtained from Air Liquide, and D_2 (D_2 2.8) from Hoekloos. These gases were effusively introduced into the 'magnetic bottle' spectrometer. In the (1+1′) REMPI experiments a molecular beam seeded with H_2 was used.

3. Molecular hydrogen and deuterium

3.1. *General considerations*

A schematic potential energy diagram containing the relevant superexcited states of molecular hydrogen is presented in figure 2. It should be noted that the electronic potential energy curves of H_2, D_2 and HD are identical to the extent that the Born–Oppenheimer approximation holds and relativistic effects can be neglected, but that vibrational and rotational manifolds are different for each isotopomer. The Born–Oppenheimer approximation, which hinges on the large difference between nuclear and electronic masses, allows the separation between nuclear and electronic motion and lies at the basis of every sensible description of molecules and molecular spectroscopy. Still, it should be realized that for molecules as 'simple' as the hydrogens this approximation is less likely to be successful than for species consisting of heavier nuclei. However, on the relatively crude scale of figure 2, deviations from the Born–Oppenheimer approximation and small effects due to relativity can be ignored.

In figure 2 the potential energy curves for the $^1\Sigma_g^+$ states with H(n = 1)+H(n = 2) and H(n = 1)+H(n = 3) dissociation limits were taken from the work of Guberman [68]. These states belong to dissociative Rydberg series converging upon the $^2\Sigma_u^+(2p\sigma_u)$ ionic limit and are designated by Q_1. The higher $^1\Sigma_g^+$ states were simply obtained by raising the R-dependent quantum defect of the $^1\Sigma_g^+$ state with the H(n = 1)+H(n = 3) dissociation limit with one for each successive state. The potential energy curves of the $^1\Pi_g$ states were calculated using the R-dependent quantum defect of the $^1\Pi_g$ state with the H(n = 1)+H(n = 2) dissociation limit. Bound singly excited Rydberg states (H_2^*(n = 3) and higher) are indicated as well. Higher-lying Rydberg states, belonging to series converging upon the $^2\Pi_u(2p\pi_u)$ ionic state (not shown), are designated by Q_2 [68]. A quasidiabatic representation is presented, ignoring the multiple interactions between singly and doubly excited Rydberg states.

For the purpose of the present study, H_2 and D_2 differ in two important aspects. First, the vibrational and rotational constants are considerably larger for the lighter molecule H_2, generally leading to rovibrational ladders associated with electronic levels with more widely spaced steps than in the case of D_2. Secondly, the two nuclei of H_2 are fermions, whereas D_2 consists of two bosons, leading to different nuclear spin

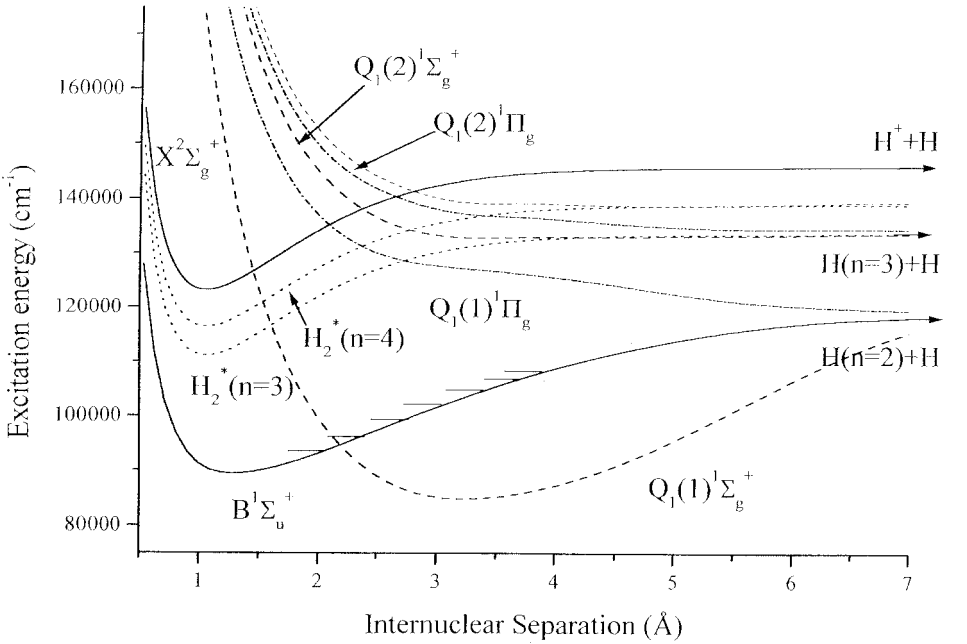

Figure 2. Schematic potential energy diagram of molecular hydrogen. The $v' = 3$–22 levels of the B $^1\Sigma_u^+$ state, accessed from the X $^1\Sigma_g^+$ ground state with three photons, are ionized directly or dissociated using a one-photon excitation via the doubly excited repulsive Q_1 states [68] of $^1\Sigma_g^+$ (– – –) or $^1\Pi_g$ symmetry (–·–) or via dissociation continua of bound singly excited Rydberg states (H_2^* ($n = 3$) and higher (·····). A quasidiabatic representation is presented, ignoring the interactions between the singly and doubly excited Rydberg states. The $v' = 3$, 5, 8, 11, 14, 17 and 20 are indicated in the B $^1\Sigma_u^+$ state. (Reproduced with permission from [35], copyright 1998 American Institute of Physics.)

statistics and hence different optical selection rules for our molecules. Ortho- and para-hydrogen, as well as ortho- and para-deuterium, can be considered as completely different molecules, with an ortho–para conversion rate which is very slow compared with the time scale of our experiments. The relevance of these issues will become apparent later.

In the following we shall discuss one-colour (3+1) REMPI–PES experiments on both H_2 and D_2, involving the three-photon transition B $^1\Sigma_u^+$ $(1s\sigma_g)(2p\sigma_u) \leftarrow\leftarrow\leftarrow$ X $^1\Sigma_g^+$ $(1s\sigma_g)^2$, and the subsequent absorption of one additional photon. Finally we shall discuss a two-colour (1+1′) REMPI experiment on H_2, in which one XUV photon induces the B $^1\Sigma_u^+$ $(1s\sigma_g)(2p\sigma_u) \leftarrow$ X $^1\Sigma_g^+$ $(1s\sigma_g)^2$ transition, with subsequent absorption of one photon from a separate tuneable laser source.

3.2. (*3+1*) *resonance-enhanced multiphoton ionization–photoelectron spectroscopy of molecular hydrogen*

In a three-photon absorption process from the X $^1\Sigma_g^+(1s\sigma_g)^2$ electronic ground state of H_2 the B $^1\Sigma_u^+$ $(1s\sigma_g)(2p\sigma_u)$($v' = 3$–22; $N' = 0$–3) levels were accessed. Excitation spectra of the B $^1\Sigma_u^+$ state were obtained by scanning the laser wavelength and by monitoring either the H^+ and H_2^+ ion channels or an energy-selected part of the electron current. The measured positions of the resonances were found to be in good agreement with literature data [69–71]. Subsequently, photoionization took place by absorption of a fourth photon. In this one-colour experiment the spectral region at the

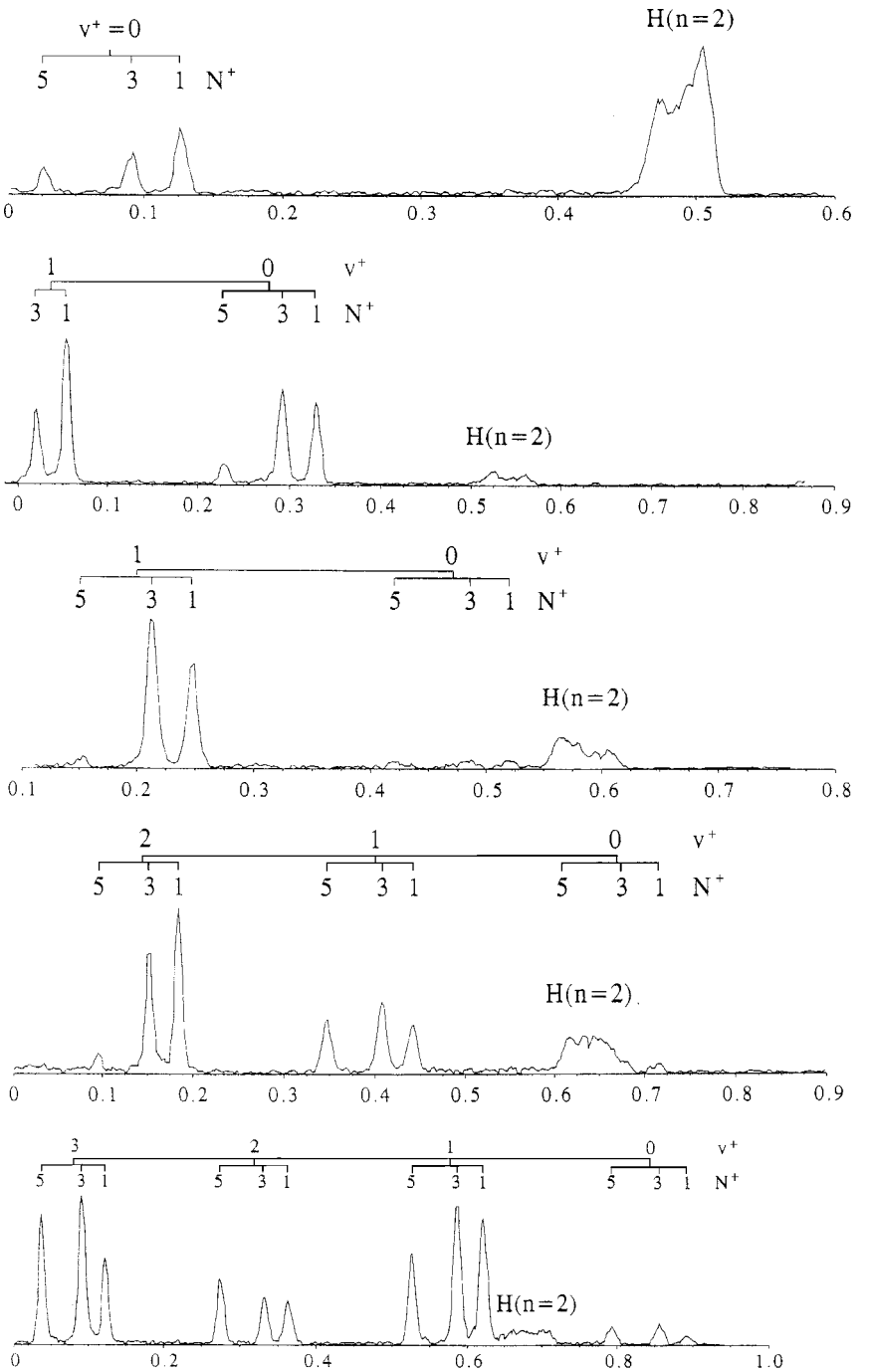

Figure 3. For legend see facing page.

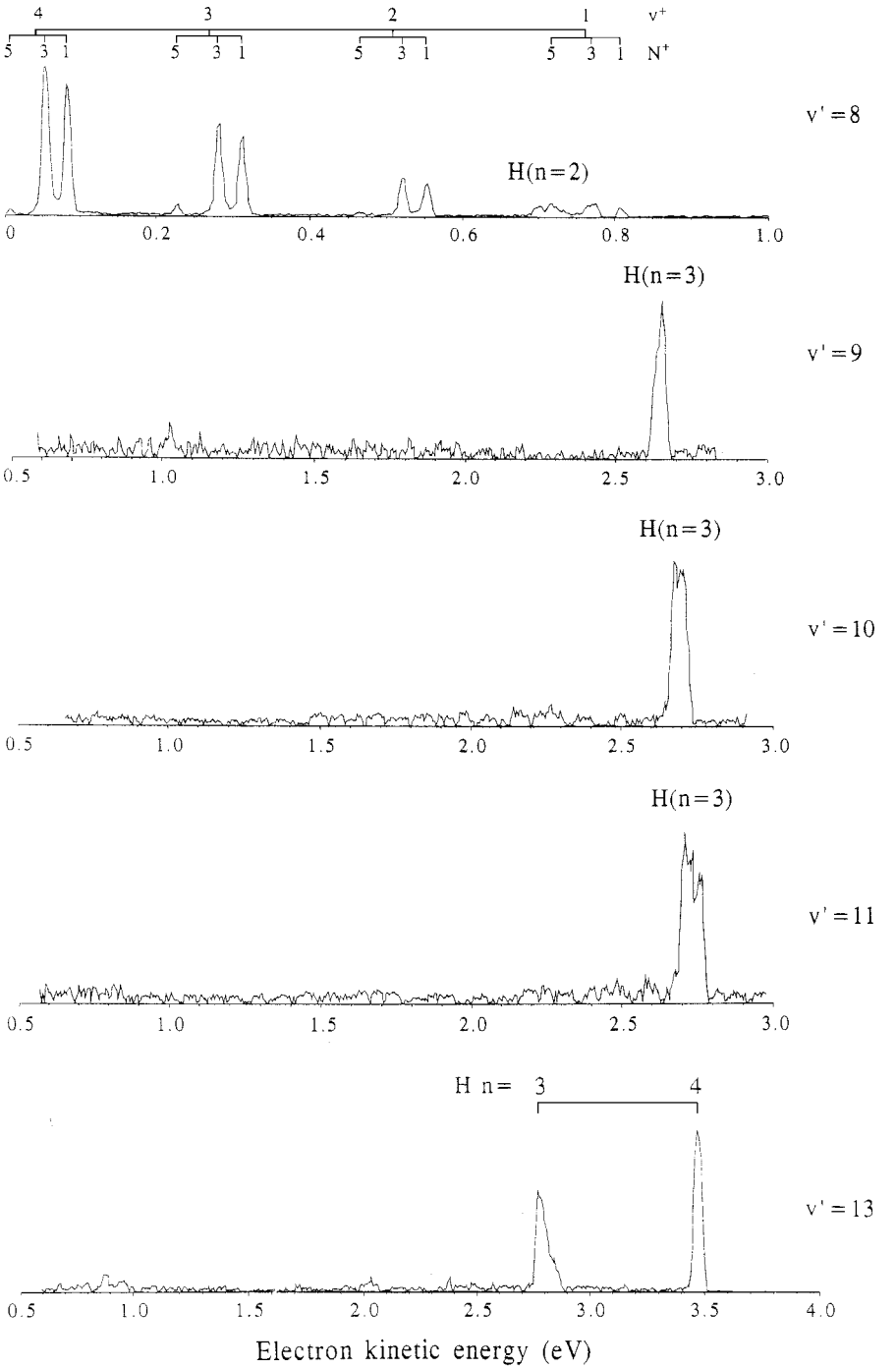

Figure 3. Laser photoelectron spectra of molecular hydrogen, obtained following three-photon excitation of the B $^1\Sigma_u^+$ (v' = 3–13) levels via the R(1) rotational transitions. (Reproduced with permission from [35], copyright 1998 American Institute of Physics.)

four-photon level, between 125000 and 150000 cm^{-1} (15.5–18.6 eV), was probed in a stepwise manner, with the steps determined by the rovibrational ladder in the B state of H_2 [35].

Photoelectron spectra were recorded following (3+1) ionization via several rotational branches associated with the $v' = 3$–22 vibrational levels. In figure 3 we select photoelectron spectra measured via the R(1) transition using $v' = 3$–13. Inspection of these spectra clearly shows that the absorption of one additional photon from B $^1\Sigma_u^+$ (v'; N') levels leads to a number of competing processes. The photoelectron spectra obtained for ionization via B $^1\Sigma_u^+$ vibrational levels $v' \leqslant 8$, for instance, are dominated by peaks arising from a molecular photoionization process, yielding H_2^+ in the various accessible vibrational (v^+) and rotational (N^+) levels of its electronic ground ionic state X $^2\Sigma_g^+$ ($1s\sigma_g$). Apart from molecular ionization, a competing dissociation process leading to excited H($n = 2$) atoms, which are subsequently ionized by absorption of one additional photon, is visible in these spectra. The width of the H($n = 2$) peak is due to the large kinetic energy (about 0.9 eV per hydrogen atom) with which the hydrogen atom fragments are formed on dissociation. It should be noted that for excitation via $v' \leqslant 8$ the four-photon energy exceeds the H($n = 1$)+H($n = 2$) energy threshold but falls short of the H($n = 1$)+H($n = 3$) limit.

For ionization via the vibrational levels $v' \leqslant 8$, dissociation plays a minor role, a situation that changes dramatically when ionization is performed via higher vibrational levels. Figure 3 shows that, above the H($n = 1$)+H($n = 3$) threshold ($v' > 8$), dissociation in fact dominates over direct ionization of molecular hydrogen, in agreement with previous results [44].

In the following we shall first discuss the molecular photoionization process, which can be observed for ionization via the vibrational levels $v' \leqslant 8$. Subsequently, the dissociation process will be considered.

3.2.1. *Molecular photoionization*

For ionization via the $v' = 3$–8 levels of the B $^1\Sigma_u^+$ state the photoelectron spectra exhibit well resolved rotational structure in the transitions deriving from molecular photoionization to the various accessible vibrational levels in the ionic ground state. Comparable structure, although far less resolved, has been observed by Dehmer *et al.* [27] for ionization via the R(3) and P(3) transitions to the $v' = 7$ level. The molecular ground and excited states involved in our experiments, as well as the lowest ionic state, all have Σ symmetry. These states can therefore be conveniently treated in a Hund's case (b) coupling scheme, in which we only focus on the end-over-end rotation N'', N' and N^+. Rotational structure in the photoelectron spectra of molecular hydrogen, ionized in a (3+1) multiphoton absorption process, is subject to rotational selection rules [72]. These selection rules predict that for one-photon ionization from the B $^1\Sigma_u^+$ (v'; N') levels, only $\Delta N + l$ = odd transitions are allowed, where $\Delta N = N^+ - N'$, and l is a partial wave component of the photoelectron. In an atomic-like picture removal of the $2p\sigma_u$ electron is expected to lead to s ($l = 0$) and d ($l = 2$) partial waves. In the photoelectron spectra, only ΔN = odd transitions would then be expected. In the B $^1\Sigma_u^+$ state, ortho-hydrogen can only exist in the $N' = 0, 2, 4, \ldots$ and para-hydrogen only in the $N' = 1, 3, 5, \ldots$ rotational levels. In the ionic X $^2\Sigma_g^+$ state, ortho-hydrogen has only $N^+ = 1, 3, 5, \ldots$ and para-hydrogen only $N^+ = 0, 2, 4 \ldots$ available to it. Therefore, in our experiments the photoelectron spectra show formation of either odd or even N^+ levels, owing to ionization of ortho- or para-hydrogen respectively.

Conservation of total angular momentum requires that s partial waves are accompanied by $\Delta N = \pm 1$, while d partial waves may lead to changes of ± 1 and ± 3. Superficially, one might be tempted to derive the relative importance of the s and d partial waves from the intensities of the $\Delta N = \pm 1$ and ± 3 transitions. The results of an *ab initio* study by Lynch *et al.* [73] of the rovibrational branching ratios resulting from (3+1) REMPI via the $v' = 7$ level of the B $^1\Sigma_u^+$ state have shown, however, that such an approach is not valid. Here it was found that $\Delta N = \pm 3$ transitions are largely suppressed as a result of dynamic interference between the $d\sigma$ and $d\pi$ channels, even though the d partial wave is in fact stronger than the s partial wave. As a result, the photoelectron spectra measured for ionization via the R(3) and P(3) transitions to the $v' = 7$ level only exhibit $\Delta N = \pm 1$ peaks.

The photoelectron spectra obtained in the present study for ionization via the $v' = 3$–8 levels of the B $^1\Sigma_u^+$ state demonstrate that the ionization dynamics as observed and calculated previously for ionization via the P(3) and R(3) transitions to the $v' = 7$ level are by no means exemplary for the other transitions. For example, figure 3 shows that, for ionization via the R(1) transition to the $v' = 3$–6 and $v' = 8$ levels, $\Delta N = \pm 3$ transitions are much weaker than $\Delta N = \pm 1$ transitions but are of similar intensity for $v' = 7$. Analogous behaviour occurs for ionizing transitions via the P(1) transition to the various vibrational levels in the excited state (not shown); ionization via the $v' = 7$ level leads to dominant intensity in the $\Delta N = \pm 3$ transitions, while these peaks are significantly less intense for ionization via other vibrational levels.

Surprisingly, the intensities of $\Delta N = \pm 3$ transitions depend not only on the initial vibrational level in the excited state but also on the rotational level, as well as on the rotational branch employed to populate this rotational level. Consider, for example, the spectra measured for ionization via the $v' = 7$ level shown in figure 4. Ionization via the P(1), R(1) and, to a lesser extent, R(0) transitions results here in significant intensities of the $\Delta N = \pm 3$ transitions, while ionization via the R(2), R(3) [43] and P(3) [43] transitions leads to dominant $\Delta N = \pm 1$ transitions. These observations are the more peculiar when it is realized that the R(1) transition, for which intense $\Delta N = \pm 3$ peaks are observed, populates the same rotational level in the excited state as the P(3) transition, where $\Delta N = \pm 3$ transitions are completely absent. Although the two rotational branches lead to a different alignment of the $N' = 2$ level, one does not expect such large differences in ionization dynamics solely on the basis of a different initial alignment.

A final striking observation is that also the vibrational branching ratios upon ionization may depend strongly on the rotational transition used to excite a particular vibrational level in the excited state. This was most apparent for ionization via the $v' = 4$ level shown in figure 5. A previous study [47] found in this case that ionization via the R(0) and P(1) transitions leads to dominant population of the $v^+ = 1$ level, while ionization via the R(1) transition results in equal intensities of the $v^+ = 0$ and $v^+ = 1$ peaks. In the present study these observations are supported and extended. Ionization via the P(2) and R(3) transitions leads to a small $v^+ = 0 : v^+ = 1$ vibrational branching ratio, ionization via the R(2) transition to a large ratio. Moreover, we observe that a large $v^+ = 0 : v^+ = 1$ branching ratio is accompanied by a significant reduction in excited H($n = 2$) fragments. Interestingly, when the photoelectron spectra are considered in order of the final energies reached in these experiments at the four-photon level, that is P(2), P(1), R(0), R(1), R(2) and R(3), it is clear that the $v^+ = 0 : v^+ = 1$ branching ratio and the amount of dissociation do not vary randomly but show a maximum and minimum respectively at around 127 100–127 150 cm^{-1}.

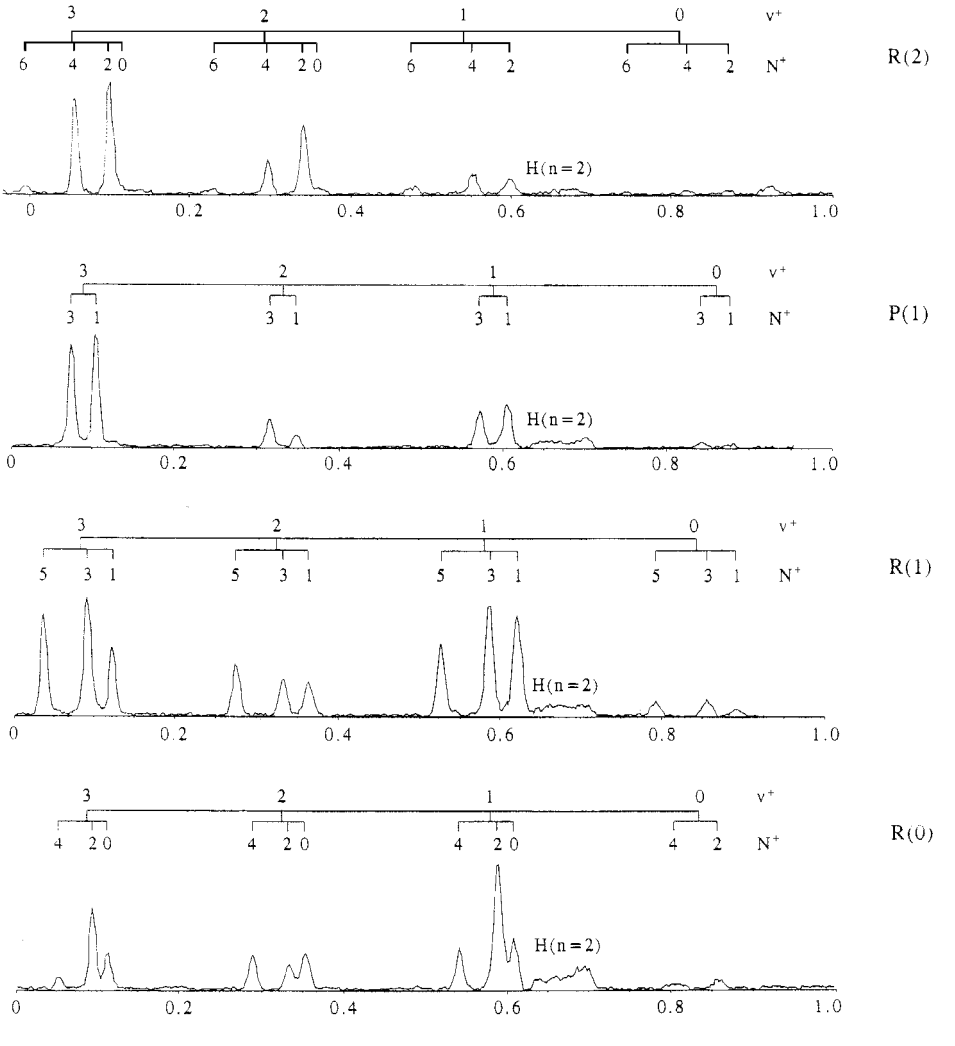

Figure 4. Laser photoelectron spectra of molecular hydrogen, obtained following three-photon excitation of the B $^1\Sigma_u^+$ ($v' = 7$) level via various rotational transitions. (Reproduced with permission from [35], copyright 1998 American Institute of Physics.)

All the above observations indicate that the ionization dynamics depend sensitively on the *four-photon* level reached in the experiments. *Ab initio* calculations have shown that dynamic interference between the dσ and dπ ionization channels plays an important role in describing ionization from the B $^1\Sigma_u^+(v' = 7)$ level [73]. The delicate balance between these two channels will certainly be dependent on the kinetic energy of the electron, but it is hard to imagine that this energy dependence would be so large that a mere change of a few 100 cm^{-1} in kinetic energy, as is occurring for example when ionizing via the R(1) or the P(3) transition to the $v' = 7$ level, would make so much difference. Another possible explanation might be found in the influence of doubly excited dissociative Rydberg states converging upon the $^2\Sigma_u^+(2p\sigma_u)$ ionic state. For excitation of the levels investigated here the only doubly excited states that can be

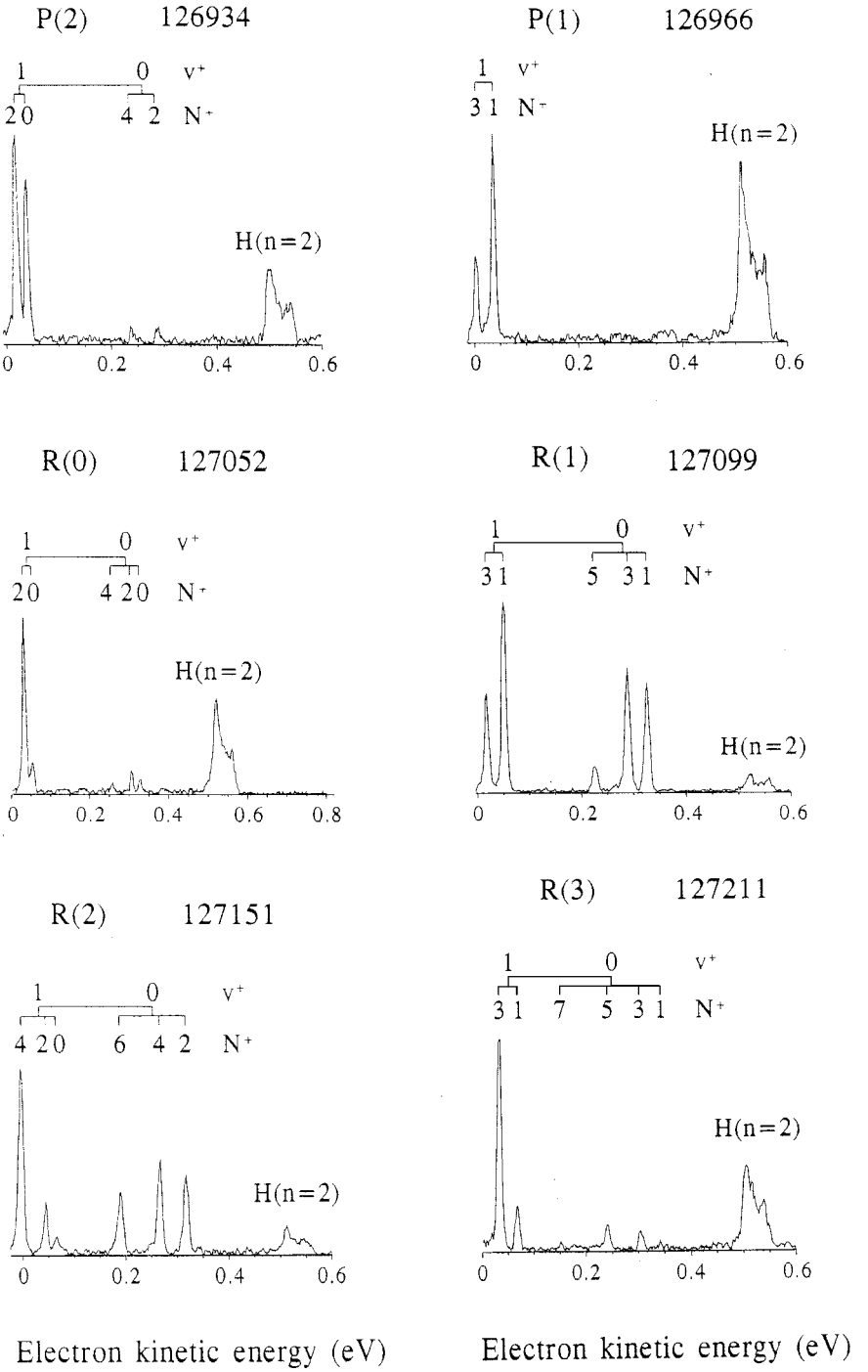

Figure 5. Laser photoelectron spectra of molecular hydrogen, obtained following three-photon excitation of the B $^1\Sigma_u^+$ ($v' = 4$) level via various rotational transitions. The final energy (cm^{-1}) reached at the four-photon level is given for each rotational transition. (Reproduced with permission from [35], copyright 1998 American Institute of Physics.)

accessed at the four-photon level are the $Q_1(1)$ $^1\Sigma_g^+$ $(2p\sigma_u)^2$ and $^1\Pi_g(2p\sigma_u)(2p\pi_u)$ Rydberg states. Calculations of the Franck–Condon factors between the vibrational wavefunctions of B $^1\Sigma_u^+(v')$ levels and these dissociative $^1\Sigma_g^+$ and $^1\Pi_g$ superexcited states show that these factors do not vary enough to account for the observed rotational branch dependence of one particular B $^1\Sigma_u^+(v')$ level. These doubly excited states might, however, be involved in an explanation of the v' dependence of the photoelectron spectra, which involve a much larger range of energies.

The fact that features observed in the photoelectron spectra change so drastically over a relatively small energy interval strongly suggests that bound states at the four-photon level should be considered. In this energy region, vibrational levels associated with singly excited Rydberg states possessing an X $^2\Sigma_g^+$ $(1s\sigma_g)$ ionic core are present. The singly excited Rydberg states which can be reached by one-photon absorption from the B $^1\Sigma_u^+$ state possess $^1\Sigma_g^+$ $(1s\sigma_g)(ns\sigma_g)$, $^1\Sigma_g^+$ $(1s\sigma_g)(nd\sigma_g)$ and $^1\Pi_g(1s\sigma_g)(nd\pi_g)$ symmetries. The excited vibrational levels associated with these Rydberg states form series of superexcited states which converge upon v^+ levels of the ground ionic state that lie higher in energy than the employed four-photon energy. From the viewpoint of vibrational overlap these levels are well accessible, since the potential energy surface of the B $^1\Sigma_u^+$ state is significantly different from that of the bound vibrational levels associated with the singly excited Rydberg states.

Upon excitation of a particular superexcited state, the photoelectron spectrum will not merely display the photoionization dynamics of the B $^1\Sigma_u^+$ state but also the decay dynamics of the bound excited vibrational level associated with a singly excited Rydberg state. A complete unravelling of the influence of bound Rydberg states on the molecular photoionization spectra clearly requires high-quality *ab initio* theoretical calculations. In addition, experimental studies, in which B $^1\Sigma_u^+$ $(v'; N')$ levels are excited by one-photon absorption and subsequently ionized in a tuneable one-photon absorption step, are very valuable as will be shown in a later section.

3.2.2. *Photodissociation*

Figure 3 shows that dissociation occurring at the four-photon level plays an important role in the one-photon excitation dynamics from the B $^1\Sigma_u^+$ state. As can be seen in the figure, for $v' \leqslant 8$, only photoionization from $H(n = 2)$ fragments is observed, which is understandable because the four-photon energy does not reach the $H(n = 1)+H(n = 3)$ threshold. As soon as this limit is exceeded for $v' = 9$, photoionization from $H(n = 3)$ fragments is observed and, curiously, the channel leading to $H(n = 2)$ is seen to close completely. For higher values of v', when hydrogen atoms in higher excited states can be produced energetically, the fragments are seen to be formed in *all* accessible excited states, with the notable exception of $H(n = 2)$. It can be shown that, under the conditions of our experiment, the ionization rates are such that all excited hydrogen atoms formed are actually ionized with a single photon. This implies that quantitative excited-atom contributions can be derived from the peak areas observed in our photoelectron spectra [35].

Our photoelectron spectra reveal that most dissociation limits are observed, once the corresponding energy threshold is exceeded at the four-photon level. A clear exception is the $H(n = 1)+H(n = 2)$ dissociation limit, which is no longer observed as soon as the production of $H(n = 3)$ becomes possible. A quantitative analysis of these fragment distributions is very complex. A logical starting point forms a calculation of the relative excitation probabilities of the different Q_1 doubly excited repulsive states. These states have Rydberg character and converge to the first excited state in H_2^+, the

$^2\Sigma_u^+$ state (see figure 2). The correlation of these states with the various dissociation limits is non-trivial. The presence of the bound singly excited Rydberg series results in a large number of (avoided) crossings. Part of the double-well structures found in Born–Oppenheimer calculations of $^1\Sigma_g^+$ Rydberg states is caused by the interactions between singly and doubly excited Rydberg states (see also the paper by Zajfman *et al.* [14]). Because of these interactions, dissociation flux will be distributed over more than one dissociation limit, even if only one doubly excited state would be excited in the Franck–Condon region.

We have attempted to model the excited atom distributions in two separate calculations:

(i) on the basis of cross-sections for one-photon excitation of the Q_1 doubly excited repulsive states, described in an uncoupled diabatic representation;
(ii) on the basis of cross-sections for one-photon excitation of the dissociation continua of singly excited Rydberg states.

Both calculations describe in zero order a one-electron transition ($nl\lambda_u \leftarrow 1s\sigma_g$) for the excitation to the doubly excited states, and ($nl\lambda_g \leftarrow 2p\sigma_u$) for excitation to the singly excited Rydberg states.

(i) We have performed approximate calculations on the relative transition probabilities for excitation from the B $^1\Sigma_u^+$ (v') levels to the one-photon accessible Q_1 $^1\Sigma_g^+$ $(2p\sigma_u)(np\sigma_u)$ and $^1\Pi_g(2p\sigma_u)(np\pi_u)$ doubly excited repulsive states possessing dissociation limits up to $n < 7$. We calculated the integrals $\int \chi_k(R)D(R)\chi_{v'}(R)\,dR$, with $\chi_k(R)$ an (energy normalized) nuclear wavefunction in the doubly excited state under consideration, $\chi_{v'}(R)$ a vibrational wavefunction of the B $^1\Sigma_u^+(v')$ level and $D(R)$ the one-photon electronic transition moment. The potential energy curves for the Q_1 $^1\Sigma_g^+$ states with H(n = 1)+H(n = 2) and H(n = 1)+H(n = 3) dissociation limits were taken from the work of Guberman [68]. Higher $^1\Sigma_g^+$ and $^1\Pi_g$ states were obtained as discussed when figure 2 was introduced. Calculations on the relevant electronic transition moment have not been published. In the one-electron approximation this transition moment is given by the $\langle 1s\sigma_g | z | 2p\sigma_u \rangle$ matrix element. These matrix elements are also the dominant contribution to the B $^1\Sigma_u^+$ $(1s\sigma_g)(2p\sigma_u)$ $\leftarrow\leftarrow\leftarrow$ X $^1\Sigma_g^+$ $(1s\sigma_g)^2$ and C $^1\Pi_u(1s\sigma_g)(2p\pi_u)\leftarrow\leftarrow\leftarrow$ X $^1\Sigma_g^+$ $(1s\sigma_g)^2$ transitions. The X–B and X–C transition moments may approximate the *magnitude* of the transition moments from the B state to the doubly excited states. The approximation becomes highly questionable at larger internuclear distances where the electronic character of the states under consideration changes. These arguments and the calculated internuclear distance dependence of the calculated X–B and X–C electronic transition moments [74] led us to use transition moments, independent of internuclear distance, of 1.6 and 1.0 au for the $^1\Sigma_g^+$ $(2p\sigma_u)^2 \leftarrow$ B $^1\Sigma_u^+$ $(1s\sigma_g)(2p\sigma_u)$ and $^1\Pi_g$ $(2p\sigma_u)(2p\pi_u) \leftarrow$ B $^1\Sigma_u^+$ $(1s\sigma_g)(2p\sigma_u)$ transitions. For transitions to the higher doubly excited states the electronic transition moments can be scaled by $(n^*/n^{**})^{3/2}$, where n^* is the effective quantum number of the $^1\Sigma_g^+$ $(2p\sigma_u)^2$ or $^1\Pi_g$ $(2p\sigma_u)(2p\pi_u)$ state, and n^{**} is the effective quantum number of the higher doubly excited state. Comparison of the distributions simulated with the above model and those obtained experimentally show poor agreement, as shown by Scheper *et al.* [35]. In particular, the simulations predict that the H(n = 2) fragments should form

an important exit channel at all four-photon energies. Simulations based upon R-dependent X–B and X–C transition moments do not improve the qualitative picture at all. Recent DR results for H_2^+ show that, at the total energies above the H(n = 3) energy, still a significant fraction of H(n = 2) fragments is found [14]. The theoretical treatment in that paper implies that the lowest $Q_1(1)$ $^1\Sigma_g^+$ state produces a significant fraction of H(n = 2) fragments at energies above the H(n = 3) limit [14]. It appears that the absence of H(n = 2) fragments above the H(n = 3) limit, observed in our experiments, cannot be explained sensibly on the basis of excitation of Q_1 doubly excited Rydberg states. This strongly suggests that another mechanism should be considered.

(ii) Above it was concluded that simulations based solely on excitation of Q_1 doubly excited Rydberg states cannot explain our experimental results. Moreover, the rapidly changing dynamics observed in the excitation from the lower B-state vibrational levels were indicative of the influence of vibrationally excited levels of singly excited Rydberg states on molecular photoionization. This prompted us to calculate the influence of the *vibrational continua* of singly excited Rydberg states with $^1\Sigma_g^+$ $(1s\sigma_g)(ns\sigma_g)$, $^1\Sigma_g^+$ $(1s\sigma_g)(nd\sigma_g)$ and $^1\Pi_g$ $(1s\sigma_g)(nd\pi_g)$ symmetries on the final fragment-state distribution. As mentioned earlier, these states can be accessed by one-photon absorption from the B $^1\Sigma_u^+$ state. We note that the potential energy curves of the B $^1\Sigma_u^+$ state differ considerably from the bound Rydberg states. Hence, the overlap between the vibrational wavefunctions of B $^1\Sigma_u^+$ (v') levels and these vibrational continua is not necessarily much smaller than the vibrational overlap for transitions to Q_1 doubly excited repulsive Rydberg states. Also, the $2p\sigma_u \rightarrow (ns\sigma_g, nd\sigma_g, nd\pi_g)$ electronic transition moments are not expected to differ vastly from the $1s\sigma_g \rightarrow (np\sigma_u, np\pi_u)$ electronic transition moments involved in the transition to doubly excited states. Excitation of these vibrational continua has been ignored in previous studies involving excitation from the B $^1\Sigma_u^+$ state, even though it was concluded to be important in one-photon excitation studies from the EF $^1\Sigma_g^+$ state [60].

To put these arguments on a somewhat more quantitative basis, we have calculated the transition moments to the vibrational continua of n = 2 and higher Rydberg states. As we observe excited hydrogen fragments, it is assumed that an $n = n'$ Rydberg state correlates with an excited H($n = n'$) fragment. Model bound Rydberg states have been constructed, assuming an R-independent integral quantum defect. Owing to a lack of better information, electronic transition moments independent of internuclear distance were also assumed. We have used the electronic transition moments calculated for the GK $^1\Sigma_g^+$ $(1s\sigma_g)(3d\sigma_g) \leftarrow$ B and H$\overline{\text{H}}$ $^1\Sigma_g^+$ $(1s\sigma_g)(3s\sigma_g) \leftarrow$ B transitions by Wolniewicz and Dressler [75], taken at the equilibrium separation of the B state. Lynch *et al.* [73] calculated for ionization of the B $^1\Sigma_u^+$ state that the electronic transition moments to the $\varepsilon s\sigma$ and $\varepsilon d\sigma$ continua are in the ratio of about 1 : 7. Since this corresponds to excitation of $n = \infty$ states, we assume that this ratio is equally applicable to the states considered here. Support for this assumption is found in the calculations of Wolniewicz and Dressler [75], where a ratio of 1 : 8 was obtained for the electronic transition moments of the GK $\leftarrow$ B and H$\overline{\text{H}} \leftarrow$ B transitions at the equilibrium distance of the B state. For transitions to Rydberg states with higher principal quantum numbers, the electronic transition moments were scaled in the same way as described for the doubly excited states. Using the Wigner–Eckart theorem it is

derived that the electronic transition moment to $n\mathrm{d}\pi_g$ states is 1.6 times smaller than that to $n\mathrm{d}\sigma_g$ states [35]. The probability for formation of H(n) is calculated by multiplying the Franck–Condon factor for excitation of the Rydberg state with the principal quantum number n by the squared transition moments to $n\mathrm{s}\sigma_g$, $n\mathrm{d}\sigma_g$ and $n\mathrm{d}\pi_g$ respectively, and by adding these contributions incoherently.

The simulation of the excited-atom distributions following from this mechanism is depicted in figure 6. The most striking difference from the previous model, based on doubly excited states, is that the contribution of H(n = 2) fragments is now absent once the H(n = 1)+H(n = 3) threshold is exceeded, in agreement with our experimental observations. Within the present model, H(n = 2) fragments can only be produced by excitation of the vibrational continuum of the EF $^1\Sigma_g^+$ state. However, our calculations indicate that the Franck–Condon factor for this pathway is negligibly small compared with excitation of the vibrational continua of n = 3 and higher Rydberg states. This calculation also suggests that the observed closing down of the molecular ionization channel for excitation via B $^1\Sigma_u^+$ ($v' > 8$) levels is due to the large cross-section for excitation of the vibrational continua of the $n \geqslant 3$ states in comparison with that for excitation of the n = 2 state. Although the dominant features observed in molecular photoionization and photodissociation are thus nicely reproduced, we note that, with this model, cross-sections for H(n = 3) production via v' = 9–11 are smaller than those calculated for H(n = 2) and H(n = 3) via the same transitions in the previous model. Although the present results strongly suggest that the vibrational continua of the bound singly excited Rydberg states play an important role in explaining our observations, quantitatively the agreement with the observed distributions is poor. This is not too surprising in view of the assumptions made. Still, we believe that our conclusions hold, even if correct R-dependent electronic transition moments were employed. A complete treatment, which would combine the excitation of doubly excited repulsive curves, the excitation of the dissociation continua of bound singly excited Rydberg states, and the interactions between singly and doubly excited Rydberg states at large internuclear separations, would clearly be very enlightening.

3.3. (3+1) *resonance-enhanced multiphoton ionization–photoelectron spectroscopy of molecular deuterium*

As discussed in the previous section, one-colour laser photoelectron spectroscopy via the B $^1\Sigma_u^+$ state of H_2 showed extensive competition at the four-photon level between molecular ionization and dissociation processes. In particular, when the four-photon energy exceeded the H(n = 1)+H(n = 3) threshold, the surprising observation was made that the production of H(n = 2) no longer occurred. Only specific four-photon energies below and above this threshold could be accessed, depending on the availability of intermediate steps provided by the rovibrational ladder associated with the B state of H_2. It was therefore considered worthwhile to study the isotopomer D_2 as well, in the four-photon energy region below and above the D(n = 1)+D(n = 3) threshold. Because of the smaller vibrational and rotational spacings between the energy levels of molecular deuterium, this can be achieved in smaller steps than in the (3+1) REMPI–PES study of molecular hydrogen. Moreover, the possible influence of the different nuclear spin statistics can be investigated [37]. In order to guide the discussion, the relevant electronic energy levels of molecular deuterium are similar to (but not identical with) those of molecular hydrogen depicted in figure 2.

In a three-photon absorption process from the X $^1\Sigma_g^+$ $(1\mathrm{s}\sigma_g)^2$ electronic ground state of D_2 the B $^1\Sigma_u^+$ $(1\mathrm{s}\sigma_g)(2\mathrm{p}\sigma_u)$($v'$ = 10–13; N' = 0–3) levels were accessed.

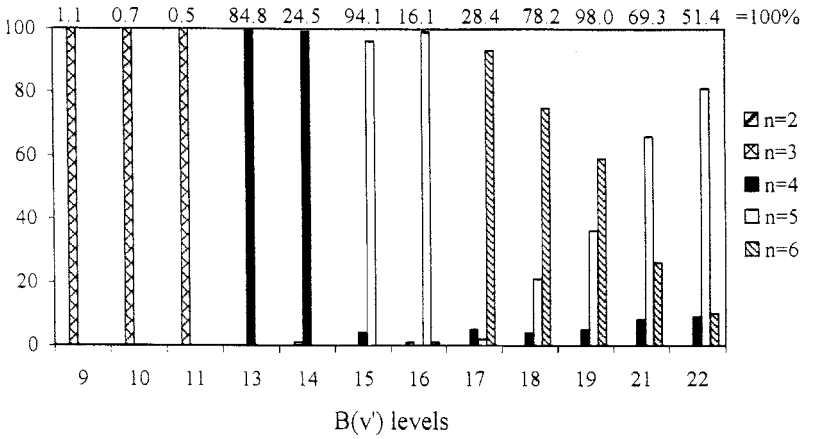

Figure 6. Excited-atom distributions H(n) calculated for three-photon excitation of molecular hydrogen via the B $^1\Sigma_u^+$ (v') levels, and assuming that dissociation uniquely occurs by one-photon excitation of the vibrational continua of bound singly excited Rydberg states with $^1\Sigma_g^+(1s\sigma_g)(ns\sigma_g)$, $^1\Sigma_g^+$ $(1s\sigma_g)(nd\sigma_g)$ and $^1\Pi_g(1s\sigma_g)(nd\pi_g)$ symmetries. For dissociation via each vibrational level the sum of the cross-sections for the pathways leading to H(n = 2) to H(n = 6) is set to 100% in the stick diagrams. The absolute value of this sum is given at the top of the diagram for each vibrational level. (Reproduced with permission from [35], copyright 1998 American Institute of Physics.)

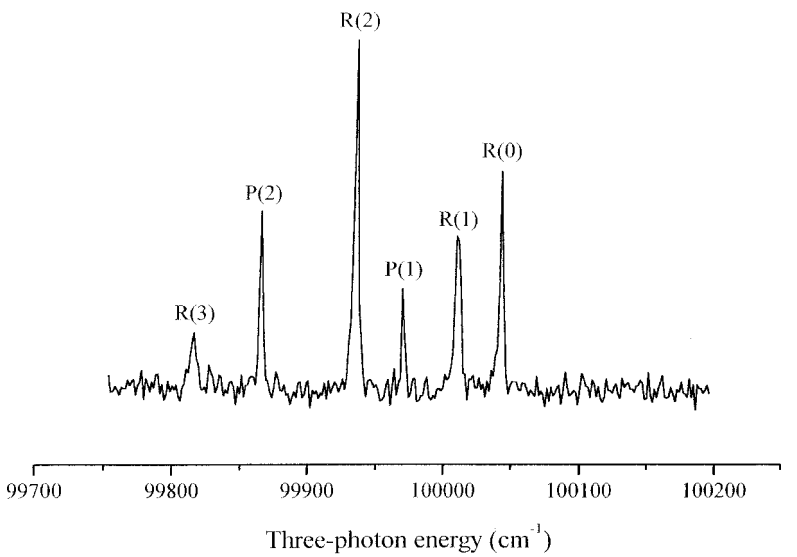

Figure 7. Three-photon excitation spectrum of molecular deuterium between the three-photon energies of 99 750 and 100 200 cm^{-1}, following the B $^1\Sigma_u^+$ $(1s\sigma_g)(2p\sigma_u)$ (v' = 11)$\leftarrow$ $\leftarrow\leftarrow$ X $^1\Sigma_g^+$ $(1s\sigma_g)^2$ transition monitored with electron detection. (Reproduced with permission from [37], copyright 2000 Elsevier Science BV.)

Subsequently, a fourth photon was absorbed. Excitation spectra of the B $^1\Sigma_u^+$ state were obtained by scanning the laser wavelength and by monitoring either the D^+ and D_2^+ ion channels, or an energy-selected part of the electron current. As an illustration a wavelength spectrum of molecular deuterium between the three-photon energies of 99 750 and 100 200 cm^{-1}, obtained with electron detection, is presented in figure 7. The

positions of the resonances in these excitation spectra agree to about 0.5 cm^{-1} with data from vacuum ultraviolet one-photon absorption spectra [70]. Assignments were taken from this previous study.

Photoelectron spectra were obtained following absorption of a fourth photon, with electrons from ionization of D_2 into the X $^2\Sigma_g^+$ (v^+; N^+) continua, either directly or through autoionization, and from subsequent one-photon ionization of excited deuterium atoms. In figure 8 a summary of photoelectron spectra obtained via B $^1\Sigma_u^+$ (v' = 10–13; N' = 0–3) and involving different rotational branches in the transition from B(v'; N') ← ← ← X(v'' = 0; N'') is presented. These spectra are organized in order of increasing three-photon energies. In addition to the molecular ionization channel, the photoelectron spectra show transitions arising from deuterium atoms formed in excited states (n = 2, 3) through photodissociation. Since in the photodissociation process, excited D(n = 2) atoms are formed with considerable excess kinetic energy (typically about 0.9 eV per deuterium atom), this is reflected in the Doppler widths of the corresponding atomic peaks. Apart from the small influence of reduced mass and of relativistic effects, which differ between hydrogen and deuterium, the excited-state energies of deuterium atoms are identical with those of hydrogen atoms. With the current resolution achievable in our photoelectron spectra, these shifts for deuterium atoms cannot be observed.

For ionization of D_2 via the vibrational levels v' = 10, 11, dissociation plays a minor role, a situation which changes dramatically when ionization is performed via higher vibrational levels. Figure 8 shows that, above the D(n = 1)+D(n = 3) threshold (for excitation via v' = 12, 13), dissociation in fact strongly dominates over direct molecular ionization. Similar to the situation in H_2, the D(n = 2) channel closes above this threshold, to be replaced by D(n = 3).

In the following we shall first discuss the molecular photoionization process, which can be observed for ionization via the vibrational levels $v' \leqslant 11$. Subsequently, the dissociation process will be considered.

3.3.1. *Molecular photoionization*

Rovibrational levels associated with the X $^1\Sigma_g^+$ (v'' = 0; N'') electronic ground state of molecular deuterium and the relevant vibrational and rotational constants are very accurately known experimentally [76]. The measured molecular transitions observed in our photoelectron spectra could easily be assigned using the results of *ab initio* calculations of the vibrational and rotational levels of molecular deuterium in its X $^2\Sigma_g^+$ ground ionic state [77]. These calculations employ the adiabatic potentials of Hunter and Pritchard [78] as their starting point and use a Numerov method to obtain vibrational and rotational levels with a numerical accuracy of better than 0.01 cm^{-1}. The agreement between the results of these computations in the adiabatic approximation and experimental data was estimated to be better than 0.1 or 0.2 cm^{-1}. The assignment procedure generally allowed a reliable determination of the rovibrational levels in X $^1\Sigma_g^+$, B $^1\Sigma_u^+$ and X $^2\Sigma_g^+$ states pertinent to the observed four-photon transition.

In the assignments of our photoelectron spectra the boson nuclear spin statistics of D_2 must be considered. In the B $^1\Sigma_u^+$ state of molecular deuterium, even values of N' can only exist in conjunction with nuclear spin wavefunctions which are antisymmetrical under permutation of the spins. Conversely, odd values of N' can only exist in combination with nuclear spin functions which are symmetrical under permutation. The ratio of symmetrical to antisymmetrical nuclear spin functions is

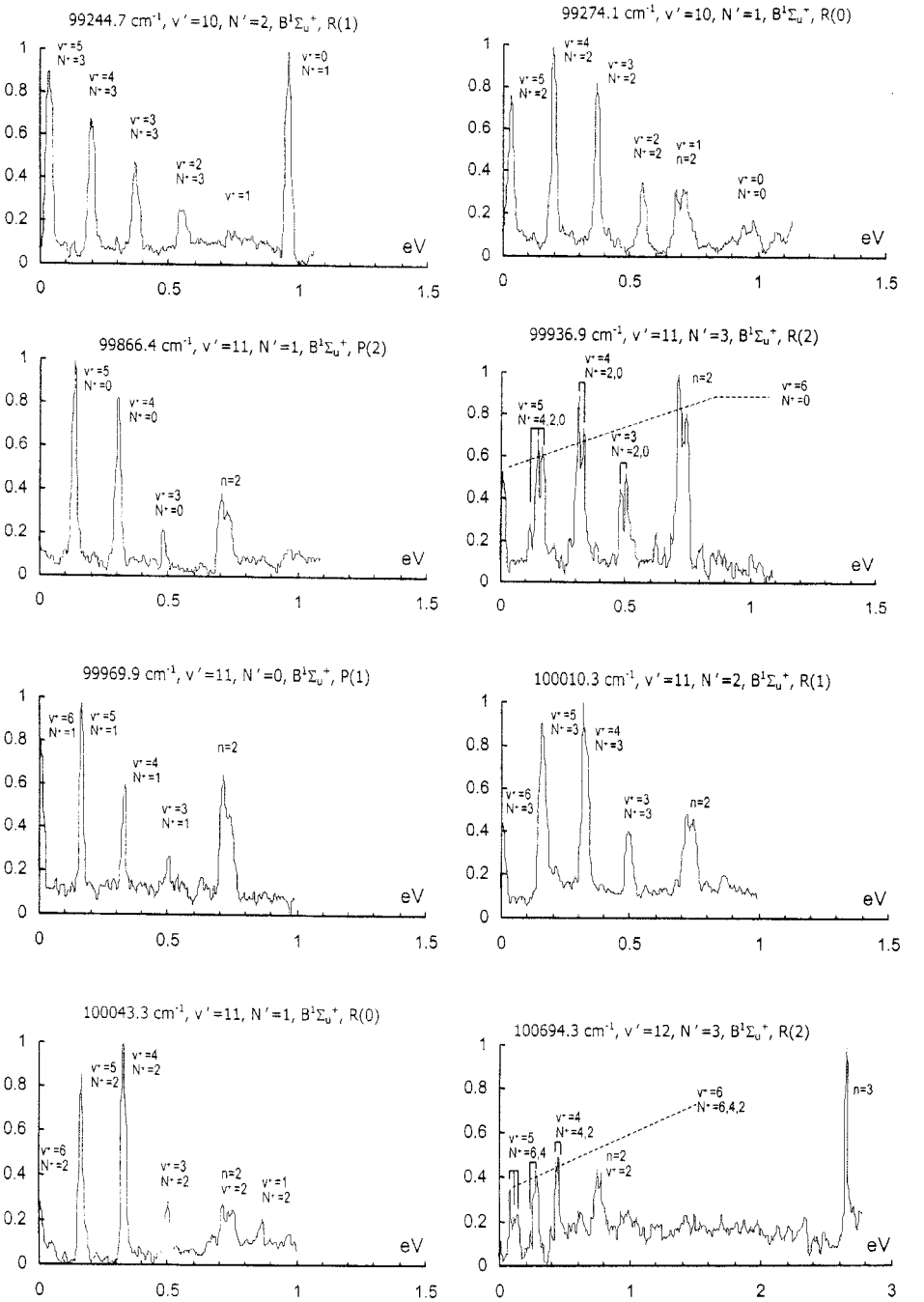

Figure 8. For legend see facing page.

2:1. In the ionic $^2\Sigma_g^+$ state of molecular deuterium, even N^+ levels exist in combination with symmetrical, odd N^+ levels with antisymmetrical nuclear spin functions. In our experiments therefore, either even or odd N^+ levels are accessed in the ionic state. In addition to the parity selection rules, conservation of angular momentum is an issue.

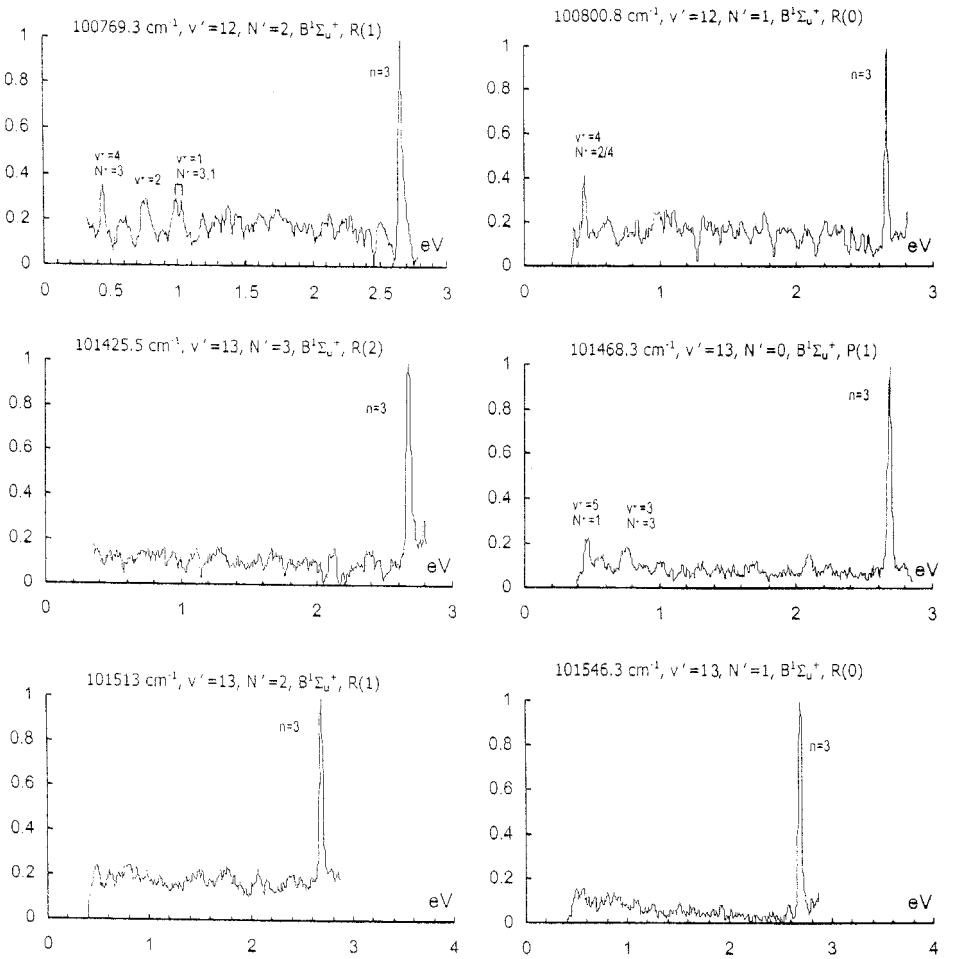

Figure 8. Laser photoelectron spectra of molecular deuterium, obtained following three-photon excitation of the B $^1\Sigma_u^+$ $(1s\sigma_g)(2p\sigma_u)$ ($v' = 10$–13) levels via various rotational transitions. The three-photon energy is given for each rotational transition. (Reproduced with permission from [37], copyright 2000 Elsevier Science BV.)

Since $\Delta N = l+1, l, \ldots, -l-1$, with the photoelectron leaving as an s partial wave, the change in overall rotation is limited to $\Delta N = \pm 1$, while for an electron leaving as a d wave $\Delta N = \pm 1, \pm 3$ holds. All our observations agree with these predictions.

When the photoelectron spectra which show significant molecular photoionization are inspected in more detail, it is apparent that, for quite small changes in the four-photon energy, very large changes in vibrational and rotational branching ratios are observed. Moreover, the relative importance of the competing molecular photoionization and photodissociation processes is also seen to vary strongly with relatively small changes in the four-photon energy. As with H_2, this behaviour is again indicative of the role played by superexcited states at the four-photon level [35].

In a few of the photoelectron spectra obtained at four-photon energies above the $D(n = 1)+D(n = 3)$ threshold (at 100 694.3, 100 769.3, 100 800.8 and 101 468.3 cm^{-1}), spectral features are observed which arise from molecular photoionization. This situation seems at odds with the statement made before that above this threshold the

molecular photoionization channel closes completely. Closer inspection shows that these molecular signals can invariably be ascribed to the close presence of levels associated with the C $^1\Pi_u$ state of D_2 [37].

In our molecular photoionization spectra, vibrational and rotational branching ratios are very dependent on small changes in the four-photon energy. Franck–Condon factors obtained with simple calculations were computed for the direct ionization process from various B $^1\Sigma_u^+(v';N')$ levels to the X $^2\Sigma_g^+(v^+)$ continua and compared with our experimental vibrational branching ratios. Although in these calculations we have neglected the changes in the electronic transition moment with internuclear distance, it was apparent that a direct photoionization process, which only allows for gradual changes in vibrational branching ratios as a function of final-state energy, could not account for our observations [37]. This situation is very similar to that encountered for molecular hydrogen previously [35]. Clearly, another mechanism, capable of explaining the fluctuations in branching ratios, as well as the variations in the competition with the photodissociation channel, is required. The explanation is again sought in the role of bound vibrationally excited states, associated with singly excited Rydberg states, and located above the lowest X $^2\Sigma_g^+$ ionic limit, but below the D(n = 1)+D(n = 3) energy threshold. These superexcited states are of electronic type $^1\Sigma_g^+(1s\sigma_g)(ns\sigma_g)$, $^1\Sigma_g^+(1s\sigma_g)(nd\sigma_g)$ and $^1\Pi_g(1s\sigma_g)(nd\pi_g)$ and form Rydberg series converging upon the lowest ionic limit. At large internuclear distances outside the Franck–Condon region these singly excited Rydberg states can couple, as before for H_2, with doubly excited dissociative Q_1 $^1\Sigma_g^+$ $(2p\sigma_u)(np\sigma_u)$ and $^1\Pi_g(2p\sigma_u)(np\pi_u)$ Rydberg states belonging to series converging upon the $^2\Sigma_u^+$ $(2p\sigma_u)$ excited ionic state. Again, depending on whether in the excitation process such a superexcited state is accessed at the four-photon level, the balance between direct molecular photoionization on the one hand, and photodissociation on the other hand, can be influenced to a very significant extent.

3.3.2. *Photodissociation*

Once the D(n = 1)+D(n = 3) threshold is exceeded in our experiments, the molecular ionization channel and the dissociation channel which involves excited D(n = 2) atoms close. Instead, the photoelectron spectra show convincing evidence for a single exit channel in which D(n = 3) is formed and subsequently ionized with one photon. These observations again are very similar in nature to what has been observed previously in our extensive (3+1) REMPI–PES study on molecular hydrogen [35]. Excitation of the vibrational continua of the $^1\Sigma_g^+$ $(1s\sigma_g)(ns\sigma_g)$, $^1\Sigma_g^+$ $(1s\sigma_g)(nd\sigma_g)$ and $^1\Pi_g(1s\sigma_g)(nd\pi_g)$ singly excited Rydberg states is again thought to play a key role in the photodissociation of molecular deuterium into the D(n = 1)+D(n = 3) channel. Clearly, for the isotopomer D_2 the nuclear spin statistics are different from the H_2 case. Also, the dissimilar vibrational and rotational constants allow for an experiment in which the energy region below and above the D(n = 1)+D(n = 3) threshold can be probed in much smaller steps than could be achieved with H_2. However, our study of D_2 shows convincingly that these differences have no bearing on the fundamental outcome of the experiments [37].

3.4. (*1+1′*) *resonance-enhanced multiphoton ionization of molecular hydrogen*

A distinct disadvantage of our (3+1) REMPI–PES experiments discussed so far is that the energy region below and above the n = 1+n = 3 limit was scanned in a stepwise manner, the magnitude of the steps being dictated by the rovibrational

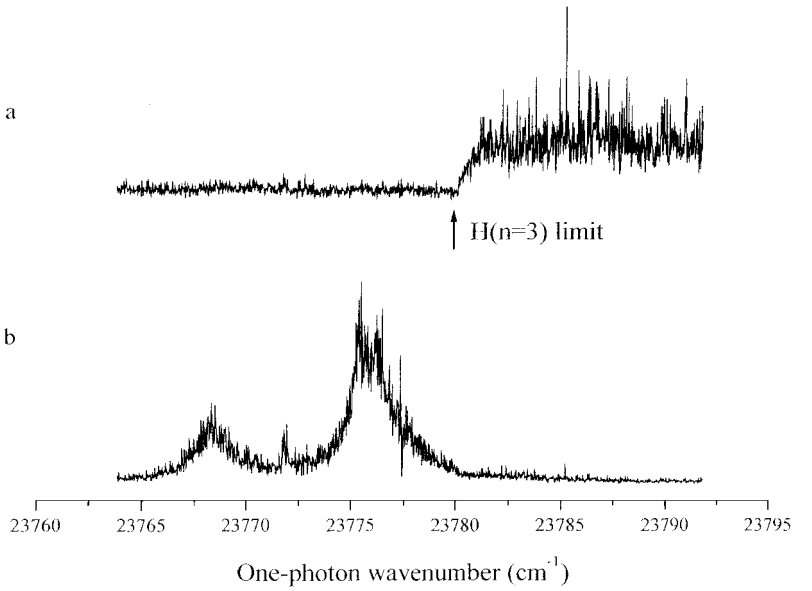

Figure 9. Two-colour (1+1′) excitation spectra of molecular hydrogen, obtained by fixing one XUV laser on the B $^1\Sigma_u^+$ ($v' = 19$; $N' = 2$) ← X $^1\Sigma_g^+$ ($v'' = 0$; $N'' = 1$) transition, while the second laser is scanned across the H($n = 1$)+H($n = 3$) dissociation limit (the frequency of the second laser is given along the horizontal axis): (*a*) the H^+ signal from ionization of $n = 3$ fragments; (*b*) the H_2^+ signal. (Reproduced with permission from [36], copyright 1999 Elsevier Science BV.)

ladders of the intermediate B state of H_2 and D_2 which was used as a stepping stone for absorption of the fourth photon. We now present an independent (1+1′) REMPI study of the H($n = 1$)+H($n = 3$) dissociation process in molecular hydrogen, in which various rovibrational levels ($v' = 19, 20$; $N' = 0, 1$) of the B $^1\Sigma_u^+$)($1s\sigma_g$)($2p\sigma_u$) state were accessed with a single XUV photon, and where the photon energy of the second photon was scanned across the $n = 3$ limit *continuously*. By monitoring the H^+ signal arising from laser-induced ionization of $n = 3$ fragments, information about the H($n = 1$)+H($n = 3$) dissociation process at this threshold was obtained [36]. The present results will again be discussed in terms of the superexcited electronic states which contribute to the H($n = 3$) yield in this energy region.

In our (1+1′) REMPI experiment we were not able to carry out photoelectron detection, and we had to resort to the detection of atomic and molecular ions. In order to observe the formation and subsequent ionization of H($n = 3$) fragments selectively, the frequency of the second photon had to fulfil certain requirements, in that its energy had to be sufficient to ionize H($n = 3$), but too small to ionize H($n = 2$). These requirements limit the frequencies which can be used for the XUV photon and restrict the vibrational levels of the B state which can be employed as stepping stones in the REMPI process. The vibrational levels used were $v' = 19$ and $v' = 20$, which are relatively high in the potential energy well of the B state. The photoexcitation process therefore addressed molecular ionization continua and superexcited states at larger internuclear distances than in the case of excitation via lower vibrational levels of the B state.

Examples of (1+1′) excitation spectra are depicted in figures 9 and 10, showing spectra for one-photon absorption from the B($v' = 19$; $N' = 2$) and the B($v' = 20$;

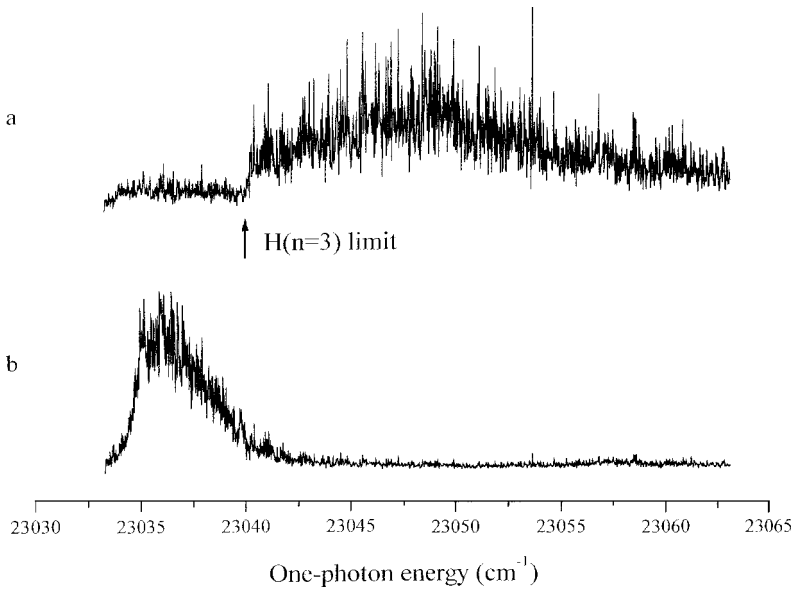

Figure 10. Two-colour (1+1′) excitation spectra of molecular hydrogen, obtained by fixing one XUV laser on the B $^1\Sigma_u^+$ ($v' = 20$; $N' = 2$) ← X $^1\Sigma_g^+$ ($v'' = 0$; $N'' = 1$) transition, while the second laser is scanned across the H($n = 1$)+H($n = 3$) dissociation limit (the frequency of the second laser is given along the horizontal axis): (*a*) the H^+ signal from ionization of $n = 3$ fragments; (*b*) the H_2^+ signal. (Reproduced with permission from [36], copyright 1999 Elsevier Science BV.)

$N' = 2$) levels respectively. The spectra obtained by monitoring the H^+ channel show a sharp onset for dissociation into H($n = 3$) fragments. The H_2^+ spectra show intense structure below the H($n = 1$)+H($n = 3$) dissociation limit, which we have not assigned. At higher excitation energies, less intense structure was observed in both H_2^+ spectra (not shown in the figures). The structure in the H_2^+ spectra arises from excitation of bound states of the neutral molecule, located above the first ionization energy. These superexcited states [32, 38, 79] can decay via autoionization and predissociation.

The measurements in figure 9 and 10 are concerned with a (1+1′) REMPI process for ortho-hydrogen starting from its X $^1\Sigma_g^+$ ($v'' = 0$; $N'' = 1$) ground state. The onset for dissociation into H($n = 3$) fragments determined from figure 9 is 23 779.91(6) cm^{-1}. The onset determined from figure 10 is 23 040.02(6) cm^{-1}. From the rotational constants of the X $^1\Sigma_g^+$ ($v'' = 0$) state [80] and the B $^1\Sigma_u^+$ ($v' = 19, 20$; $N' = 2$) ← X $^1\Sigma_g^+$ ($v'' = 0$; $N'' = 1$) transition frequencies [81, 82], it can be calculated that the formation of H($n = 3$) fragments must occur at 133 610.28(6) or 133 610.34(6) cm^{-1}, above the X $^1\Sigma_g^+$ ($v'' = 0$; $N'' = 0$) ground state, based on the onsets measured in figure 9 and 10. The onset determined for one-photon absorption from the B($v' = 20$; $N' = 1$) level, excited from the ground state of para-hydrogen, is 133 610.13(10) cm^{-1}. By using results from [80–82], it was calculated that the excitation energy required to reach the H($n = 1$)+H($n = 3$) dissociation limit from the X $^1\Sigma_g^+$ ($v'' = 0$; $N'' = 0$) level ranges from 133 610.27 to 133 610.41 cm^{-1} for the various fine structure levels of the H($n = 3$) fragments. From our results, it can be concluded that H($n = 3$) fragments were observed at *precisely* the energy at which the H($n = 1$)+H($n = 3$) dissociation threshold was surpassed.

The initial distribution of the H(3*l*) atoms over the various angular momentum substates is *a priori* unknown in our experiments. During the applied waiting period, the various H(3*l*) atoms were also subject to radiative decay and possibly collisional deactivation processes with different transition probabilities. From the radiative lifetimes of the 3s, 3p and 3d states [83], it can be estimated that, after the applied delay time of 20 ns, 88% of the 3s, 2.5% of the 3p and 28% of the 3d atoms will remain. The initial populations of the various angular momentum substates of H(n = 3) atoms, resulting from excitation between the H(n = 1)+H(n = 3) and the H(n = 1)+H(n = 4) dissociation limits by one-photon absorption from the X $^1\Sigma_g^+$ electronic ground state, have been determined experimentally by Kouchi *et al.* [84] and Terazawa *et al.* [85] by analysis of the observed time-dependent Balmer α intensity. In these experiments, states of *ungerade* symmetry are excited while, in the present experiments *gerade* states were accessed. These experimental results are therefore not directly applicable, but we can conclude that the observed H^+ signal mainly results from ionization of 3s and 3d atoms, which have survived radiative decay during the delay period. The experimental errors are, however, too large to distinguish between these two dissociation limits.

The onset of H(1s)+H(3*l*λ) dissociation channels in the present experiment is influenced by the atomic interaction potentials V_a as calculated by Stephens and Dalgarno [86], as well as by a centrifugal term V_c for continua with $J > 0$. The centrifugal barrier in the effective radial potential arising from the centrifugal term can be calculated as the maximum of the sum of V_a and V_c. Note that, unlike the neutral ground X $^1\Sigma_g^+(1s\sigma_g)^2$, the neutral excited B $^1\Sigma_u^+$ and the lowest ionic X $^2\Sigma_g^+(1s\sigma_g)$ states involved in our experiments, electronic continuum states with symmetry other than Σ, which do not conform to Hund's case (b) coupling scheme, can also occur here. In those cases the total angular momentum J should be considered.

All 3s and 3d configurations are dominated by attractive van der Waals interaction, although the 3d configurations contain a small quadrupolar term as well. In contrast, the strongest contributions to the 3p potentials are dipolar interaction terms. The interaction is repulsive for the 3pσ, excluding this configuration from near-threshold dissociation. The 3pπ and 3dπ configurations are restricted to continuum states with $J \geqslant 1$; excitation of the 3dδ configuration from the intermediate B $^1\Sigma_u^+$ state is impossible owing to dipole selection rules. Therefore, 3sσ and 3dσ configurations may contribute to dissociation continua with total angular momentum $J = 0$, excited via an $N' = 1$ intermediate state.

In continua with non-zero angular momentum of nuclear motion the centrifugal term $V_c = [J(J+1) - \Lambda^2]/2\mu R^2$ (V and R in atomic units) give rise to a barrier in the effective radial potential. For $J = 1$ continuum states, the lowest possible value accessed via $N' = 2$ intermediate states, the resulting centrifugal barrier heights are 0.10 cm^{-1} (3sσ), 0.11 cm^{-1} (3dσ), 0.0006 cm^{-1} (3pπ) and 0.04 cm^{-1} (3dπ). Continua with $J > 1$ show centrifugal barriers of more than 0.5 cm^{-1}, except for the 3pπ configuration with 0.08 cm^{-1} for $J = 2$. However, even at energies below the barrier but above the dissociation energy, tunnelling can still lead to dissociation. The dissociation probability p increases smoothly with the energy ε above threshold, quantified by Wigner's threshold law $p \propto \varepsilon^{J+1/2}$. Therefore, the presence of centrifugal barriers may shift the onset of dissociation towards higher energies by no more than 0.05 cm^{-1}, as observed from linear fits to signals arising from the intermediate states with $N' = 2$ (see figures 9 and 10).

In figure 11, the H^+ and H_2^+ spectra are depicted for one-photon absorption from

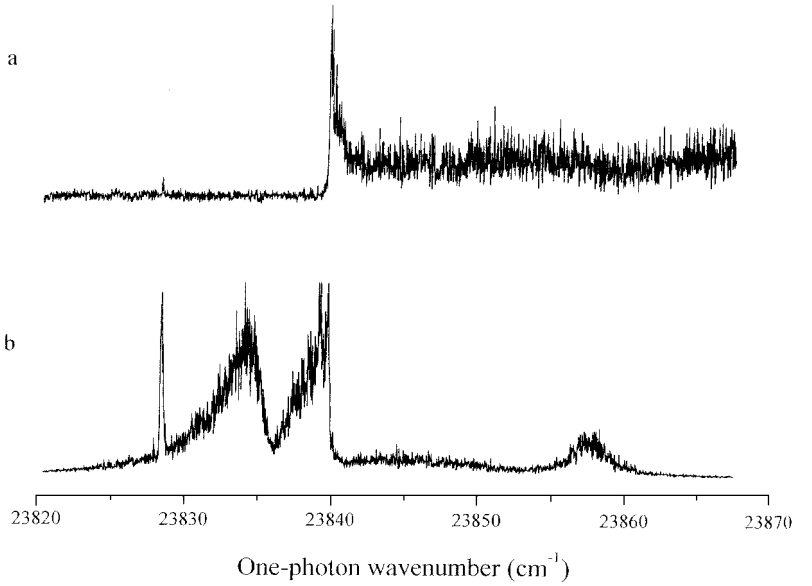

Figure 11. Two-colour (1+1′) excitation spectra of molecular hydrogen, obtained by fixing one XUV laser on the B $^1\Sigma_u^+$ ($v' = 19$; $N' = 0$) ← $^1\Sigma_g^+$ ($v'' = 0$; $N'' = 1$) transition, while the second laser is scanned across the H($n = 1$)+H($n = 3$) dissociation limit (the frequency of the second laser is given along the horizontal axis): (*a*) the H^+ signal from ionization of $n = 3$ fragments; (*b*) the H^+_2 signal. This example clearly shows the closing of the autoionization channel on a broad resonance of H_2 at the H($n = 3$) limit. (Reproduced with permission from [36], copyright 1999 Elsevier Science BV.)

the B($v' = 19; N' = 0$) level. These spectra show that at the H($n = 1$)+H($n = 3$) dissociation threshold the autoionization channel closes, to be replaced by dissociation into H($n = 1$) and H($n = 3$) fragments. This observation is in agreement with the results from one-colour (3+1) REMPI–PES experiments in which dissociation dominates over ionization of molecular hydrogen above the H($n = 1$)+H($n = 3$) dissociation limit [35, 44, 46]. However, at a one-photon energy of 23858 cm^{-1}, which corresponds to an energy of 133630 cm^{-1} above the X $^1\Sigma_g^+$($v'' = 0; N'' = 0$) ground state, some structure was still observed in the H_2^+ channel.

Following one-photon absorption from the B $^1\Sigma_u^+$ state, excitation of doubly excited dissociative states with $^1\Sigma_g^+(2p\sigma_u)(np\sigma_u)$ and $^1\Pi_g(2p\sigma_u)(np\pi_u)$ configurations should be considered. Excitation of the $Q_1(2)$ $(2p\sigma_u)(3p\sigma_u)$ or the $Q_1(2)$ $(2p\sigma_u)(3p\pi_u)$ state may lead to dissociation into H($n = 3$) fragments. The $(2p\sigma_u)(3p\pi_u)$ potential is repulsive at all internuclear separations R. As a consequence, for a transition from any bound state into the dissociative continuum the Franck–Condon factor vanishes as the excitation energy approaches the dissociation threshold. In contrast, the $(2p\sigma_u)(3p\sigma_u)$ potential is slightly bound with respect to the H($n = 1$)+H($n = 3$) dissociation limit for $R > 6$ au [68], giving rise to some Franck–Condon overlap with the long-range part of the B ($v' = 19$) and B($v' = 20$) potential energy curves, with an outer classical turning point of about 8 au.

However, the preferred explanation for the observation of $n = 3$ fragments in this energy region involves the excitation of vibrational continua of singly excited Rydberg states with $^1\Sigma_g^+(1s\sigma_g)(ns\sigma_g)$, $^1\Sigma_g^+(1s\sigma_g)(nd\sigma_g)$ and $^1\Pi_g(1s\sigma_g)(nd\pi_g)$ configurations, converging upon the ground ionic state X $^2\Sigma_g^+(1s\sigma_g)$. As discussed before, excitation

of vibrational continua of those Rydberg states which possess a H(n = 1)+H(n = 3) dissociation limit results in the observation of H(n = 3) fragments. In a diabatic picture, the dissociation of the molecule following excitation of the doubly excited $Q_1(1)\ ^1\Sigma_g^+\ (2p\sigma_u)^2$ or $Q_1(1)\ ^1\Pi_g(2p\sigma_u)(2p\pi_u)$ states results in H(n = 2) excited fragments. Interaction with Rydberg states that exhibit (diabatic) potential crossings with the doubly excited states, however, may redistribute the flux in the various exit channels. This has been observed in DR experiments where exclusive population of the $Q_1(1)\ ^1\Sigma_g^+(2p\sigma_u)^2$ state leads to considerable population in all energetically allowed dissociation channels [14]. Since our (3+1) REMPI–PES experiments have shown unambiguously that H(n = 2) dissociation products completely disappear above the H(n = 1)+H(n = 3) dissociation limit [35, 46], the dissociation into H(n = 3) fragments via the dissociation mechanism which involves doubly excited states with a H(n = 1)+H(n = 2) dissociation limit can be excluded.

The interpretation of our experimental results in terms of vibrational continua of singly excited Rydberg states is supported by experiments in which the Balmer α radiation of H(n = 3) fragments was monitored as a function of the excitation wavelength [87] (M. Ukai 1999, private communication). This radiation was observed as soon as the H(n = 3) dissociation threshold is reached by one-photon absorption from the $X\ ^1\Sigma_g^+$ ground state. In this way, *ungerade* states are excited at small internuclear distances, so that doubly excited states with a H(n = 1)+H(n = 3) dissociation limit cannot be accessed at these excitation energies. This can be viewed as another indication of the importance of the vibrational continua of singly excited bound Rydberg states in the dissociation process.

4. Conclusions

In DR of H_2^+, D_2^+ and HD^+ the role of doubly excited repulsive Rydberg states in the so-called direct process and that of vibrationally excited singly excited bound Rydberg states in a so-called indirect process have been a matter of considerable debate. The doubly excited repulsive Rydberg states, which are usually considered, possess configurations $(2p\sigma_u)(nl\lambda)$, forming Rydberg series converging upon the $^2\Sigma_u^+(2p\sigma_u)$ ionic limit, or, at higher energies, have configurations $(2p\pi_u)(nl\lambda)$, leading to series converging upon the $^2\Pi_u(2p\pi_u)$ ionic state. The singly excited bound Rydberg state possess configurations $(1s\sigma_g)(nl\lambda)$ and form Rydberg series converging upon the $X\ ^2\Sigma_g^+(1s\sigma_g)$ ionic threshold. In order to elucidate the role of these superexcited states in molecular dissociation, experiments via the $B\ ^1\Sigma_u^+$ intermediate state were carried out on H_2 and D_2 with (3+1) one-colour laser photoelectron spectroscopy, and on H_2 with (1+1′) two-colour REMPI. In all these experiments it was apparent that, as soon as the H(n = 1)+H(n = 3) dissociation threshold was energetically exceeded, the formation of molecular ions and of excited H(n = 2) fragments was virtually terminated, to be replaced by the abundant generation of H(n = 3) fragments. When higher H(n = 1)+H($n \geqslant 3$) dissociation thresholds were surpassed, a variety of excited hydrogen atoms distributed over the available H($n \geqslant 3$) channels was observed. In particular, in the (1+1′) REMPI experiment, in which the $B\ ^1\Sigma_u^+$ state was excited with a XUV photon, and where the H(n = 1)+H(n = 3) dissociation threshold was scanned continuously with a second photon, we focused on the formation of H(n = 3) fragments.

In order to explain our combined observations, two mechanisms consistent with all our experiments can be proposed. The formation of H(n = 3) fragments at the H(n = 1)+H(n = 3) dissociation threshold and at energies just above this limit either

originates from the long-range part of a higher doubly excited repulsive state or results from direct excitation of vibrational continua of singly excited Rydberg states. However, when model calculations as well as experimental data from other research groups are taken into consideration, cumulative evidence leads us to conclude that a very significant contribution to the production of H(n = 3) fragments at the H(n = 1)+H(n = 3) dissociation threshold originates from the direct excitation of vibrational continua of singly excited Rydberg states.

Acknowledgements

The invaluable contributions of Arno de Lange, Elmar Reinhold, Connie Scheper, Mark Somers and of senior colleagues Wim Ubachs and Wim van der Zande are gratefully acknowledged. Discussions with Professor Masatoshi Ukai have been particularly enlightening.

References

[1] Adams, N. G., 1993, *Dissociative Recombination: Theory, Experiment and Applications*, edited by B. R. Rowe, J. B. A. Mitchell and A. Canosa (New York: Plenum), p. 99.
[2] Rowe, B. R., 1993, *Dissociative Recombination: Theory, Experiment and Applications*, edited by B. R. Rowe, J. B. A. Mitchell and A. Canosa (New York: Plenum), p. 113.
[3] Peart, B., and Dolder, K. T., 1974, *J. Phys.* B, **7**, 236.
[4] Mathur, D., Khan, S. U., and Hasted, J. B., 1978, *J. Phys.* B, **11**, 3615.
[5] Auerbach, D., Cacak, R., Caudano, R., Gaily, T. D., Keyser, C. J., McGowan, J. W., Mitchell, J. B. A., and Wilk, S. F. J., 1977, *J. Phys.* B, **10**, 3797.
[6] Mitchell, J. B. A., Yousif, F. B., Van der Donk, P., and Morgan, T. J., 1993, *Dissociative Recombination: Theory, Experiment and Applications*, edited by B. R. Rowe, J. B. A. Mitchell and A. Canosa (New York: Plenum), p. 87.
[7] Van der Donk, P., Yousif, F. B., Mitchell, J. B. A., and Hickman, A. P., 1991, *Phys. Rev. Lett.*, **67**, 42.
[8] Larsson, M., 1997, *A. Rev. phys. Chem.*, **48**, 151.
[9] Forck, P., Grieser, M., Habs, D., Lampert, A., Repnow, R., Schwalm, D., Wolf, A., and Zajfman, D., 1993, *Phys. Rev. Lett.*, **70**, 426.
[10] Larsson, M., Carlson, M., Danared, H., Broström, L., Mannervik, S., and Sundström, G., 1994, *J. Phys.* B, **27**, 1397.
[11] Zajfman, D., Amitay, Z., Broudem, C., Forck, P., Seidel, B., Grieser, M., Habs, D., Schwalm, D., and Wolf, A., 1995, *Phys. Rev. Lett.*, **75**, 814.
[12] Strömholm, C., Schneider, I. F., Sundström, G., Carata, L., Danared, H., Datz, S., Dulieu, O., Källberg, A., af Ugglas, M., Urbain, X., Zengin, V., Suzor-Weiner, A., and Larsson, M., 1995, *Phys. Rev.* A, **52**, R4320.
[13] Van der Zande, W. J., Semaniak, J., Zengin, V., Sundström, G., Rosén, S., Strömholm, C., Datz, S., Danared, H., and Larsson, M., 1996, *Phys. Rev.* A, **54**, 5010.
[14] Zajfman, D., Amitay, Z., Lange, M., Hechtfischer, U., Knoll, L., Schwalm, D., Wester, R., Wolf, A., and Urbain, X., 1997, *Phys. Rev. Lett.*, **79**, 1829.
[15] Bates, D. R., 1950, *Phys. Rev.*, **78**, 492.
[16] Bardsley, J. N., 1968, *J. Phys.* B, **1**, 365.
[17] Chupka, W. A., 1987, *J. chem. Phys.*, **87**, 1488.
[18] Giusti-Suzor, A., Bardsley, J. N., and Derkits, C., 1983, *Phys. Rev.* A, **28**, 682.
[19] Seaton, M. J., 1983, *Prog. Phys.*, **46**, 167.
[20] Greene, C. H., and Jungen, Ch., 1985, *Adv. at. molec. Phys.*, **21**, 51.
[21] Schneider, I. F., Dulieu, O., and Giusti-Suzor, A., 1991, *J. Phys.* B, **24**, L289.
[22] Voronov, G. S., and Delone, N. B., 1966, *Soviet Phys. JETP*, **23**, 54.
[23] Lin, S. H., Fujimura, Y., Neusser, H. J., and Schlag, E. W., 1984, *Multiphoton Spectroscopy of Molecules* (New York: Academic Press).
[24] Reilly, J. P., 1984, *Israel J. Chem.*, **24**, 266.
[25] Kimura, K., 1985, *Adv. chem. Phys.*, **60**, 161.
[26] Kimura, K., 1987, *Int. Rev. phys. Chem.*, **6**, 195.
[27] Dehmer, P. M., Dehmer, J. L., and Pratt, S. T., 1987, *Comments at. molec. Phys.*, **19**, 205.

[28] PRATT, S. T., DEHMER, P. M., and DEHMER, J. L., 1988, *Advances in Multiphoton Processes and Spectroscopy*, Vol. 4, edited by S. H. Lin (Singapore: World Scientific Press).
[29] COMPTON, R. N., and MILLER, J. C., 1989, *Laser Applications in Physical Chemistry*, edited by D. K. Evans (New York: Marcel Dekker), p. 121.
[30] MILAN, J. B., BUMA, W. J., DE LANGE, C. A., WESTERN, C. M., and ASHFOLD, M. N. R., 1995, *Chem. Phys. Lett.*, **239**, 326.
[31] MILAN, J. B., BUMA, W. J., and DE LANGE, C. A., 1996, *J. chem. Phys.*, **105**, 6688.
[32] DE LANGE, C. A., 1998, *J. chem. Soc., Faraday Trans.*, **94**, 3409.
[33] DE LANGE, C. A., 1999, *The Role of Rydberg States in Spectroscopy and Reactivity*, edited by C. Sandorfy (Deventer: Kluwer), p. 457.
[34] DOBBER, M. R., BUMA, W. J., and DE LANGE, C. A., 1994, *J. chem. Phys.*, **101**, 9303.
[35] SCHEPER, C. R., BUMA, W. J., DE LANGE, C. A., and VAN DER ZANDE, W. J., 1998, *J. chem. Phys.*, **109**, 8319.
[36] SCHEPER, C. R., DE LANGE, C. A., DE LANGE, A., REINHOLD, E., and UBACHS, W., 1999, *Chem. Phys. Lett.*, **312**, 131.
[37] SCHEPER, C. R., SOMERS, M. F., and DE LANGE, C. A., 2000, *J. Electron Spectrosc. Related Phenomena*, **108**, 123.
[38] DE LANGE, C. A., 2001, *Adv. chem. Phys.* (to be published).
[39] KRUIT, P., and READ, F. H., 1983, *J. Phys.* E, **16**, 313.
[40] KOENDERS, B. G., WIERINGA, D. M., DRABE, K. E., and DE LANGE, C. A., 1987, *Chem. Phys.*, **118**, 113.
[41] DE LANGE, C. A., 1995, *High Resolution Laser Photoionization and Photoelectron Studies*, edited by I. Powis, T. Baer and C. Y. Ng (New York: Wiley), p. 195.
[42] RIJS, A. M., BACKUS, E. H. G., DE LANGE, C. A., WESTWOOD, N. P. C., and JANSSEN, M. H. M., 2000, *J. Electron Spectrosc. Related Phenomena* (to be published).
[43] PRATT, S. T., DEHMER, P. M., and DEHMER, J. L., 1983, *J. chem. Phys.*, **78**, 4315.
[44] BONNIE, J. H. M., VERSCHUUR, J. W. J., HOPMAN, H. J., and VAN LINDEN VAN DEN HEUVELL, H. B., 1986, *Chem. Phys. Lett.*, **130**, 43.
[45] XU, E. Y., TSUBOI, T., KACHRU, R., and HELM, H., 1987, *Phys. Rev.* A, **36**, 5645.
[46] VERSCHUUR, J. W. J., NOORDAM, L. D., BONNIE, J. H. M., and VAN LINDEN VAN DEN HEUVELL, H. B., 1988, *Chem. Phys. Lett.*, **146**, 283.
[47] VERSCHUUR, J. W. J., and VAN LINDEN VAN DEN HEUVELL, H. B., 1989, *Chem. Phys.*, **129**, 1.
[48] PRATT, S. T., DEHMER, P. M., and DEHMER, J. L., 1984, *Chem. Phys. Lett.*, **105**, 28.
[49] PRATT, S. T., DEHMER, P. M., and DEHMER, J. L., 1986, *J. chem. Phys.*, **85**, 3379.
[50] O'HALLORAN, M. A., PRATT, S. T., DEHMER, P. M., and DEHMER, J. L., 1987, *J. chem. Phys.*, **87**, 3288.
[51] PRATT, S. T., DEHMER, P. M., and DEHMER, J. L., 1987, *J. chem. Phys.*, **87**, 4423.
[52] ZUCKER, C. W., and EYLER, E. E., 1986, *J. chem. Phys.*, **85**, 7180.
[53] NORMAND, D., CORNAGGIA, C., and MORELLEC, J., 1986, *J. Phys.* B, **19**, 2881.
[54] CORNAGGIA, C., NORMAND, D., MORELLEC, J., MAINFRAY, G., and MANUS, C., 1986, *Phys. Rev.* A, **34**, 207.
[55] GLAB, W. L., and HESSLER, J. P., 1987, *Phys. Rev.* A, **35**, 2102.
[56] BUCK, J. D., ROBIE, D. C., HICKMAN, A. P., BAMFORD, D. J., and BISCHEL, W. K., 1989, *Phys. Rev.* A, **39**, 3932.
[57] XU, E. Y., HELM, H., and KACHRU, R., 1989, *Phys. Rev.* A, **39**, 3979.
[58] XU, E., HICKMAN, A. P., KACHRU, R., TSUBOI, T., and HELM, H., 1989, *Phys. Rev.*, A, **40**, 7031.
[59] BUNTINE, M. A., BALDWIN, D. P., and CHANDLER, D. W., 1992, *J. chem. Phys.*, **96**, 5843.
[60] MCCORMACK, E. F., PRATT, S. T., DEHMER, P. M., and DEHMER, J. L., 1993, *J. chem. Phys.*, **98**, 8370.
[61] PRATT, S. T., DEHMER, P. M., and DEHMER, J. L., 1987, *J. chem. Phys.*, **86**, 1727.
[62] MILAN, J. B., BUMA, W. J., and DE LANGE, C. A., 1996, *J. chem. Phys.*, **104**, 521.
[63] UBACHS, W., EIKEMA, K. S. E., and HOGERVORST, W., 1993, *Appl. Phys.* B, **57**, 411.
[64] HINNEN, P. C., 1997, PhD thesis, Vrije Universiteit, Amsterdam.
[65] HINNEN, P. C., HOGERVORST, W., STOLTE, S., and UBACHS, W., 1994, *Can. J. Phys.*, **72**, 1032.
[66] REINHOLD, E., HOGERVORST, W., and UBACHS, W., 1996, *J. molec. Spectrosc.*, **180**, 156.

[67] CARIOU, J., and LUC, P., 1980, *Atlas du Spectre d'Absorption de la Molécule de Tellure* (Orsay: CNRS).
[68] GUBERMAN, S. L., 1983, *J. chem. Phys.*, **78**, 1404.
[69] WILKINSON, P. G., 1968, *Can J. Phys.*, **46**, 1225.
[70] DABROWSKI, I., and HERZBERG, G., 1974, *Can. J. Phys.*, **52**, 1110.
[71] NAMIOKA, T., 1964, *J. chem. Phys.*, **40**, 3154.
[72] XIE, J., and ZARE, R. N., 1990, *J. chem. Phys.*, **93**, 3033.
[73] LYNCH, D. L., DIXIT, S. N., and MCKOY, V., 1986, *Chem. Phys. Lett.*, **123**, 315.
[74] WOLNIEWICZ, L., 1969, *J. chem. Phys.*, **51**, 5002.
[75] WOLNIEWICZ, L., and DRESSLER, K., 1982, *J. molec. Spectrosc.*, **96**, 195.
[76] HUBER, K. P., and HERZBERG, G., 1979, *Molecular Spectra and Molecular Structure*, Vol. IV, *Constants of Diatomic Molecules* (New York: Van Nostrand Reinhold).
[77] HUNTER, G., YAU, A. W., and PRITCHARD, H. O., 1974, *At. Data nucl. Data Tables*, **14**, 1.
[78] HUNTER, G., and PRITCHARD, H. O., 1967, *J. chem. Phys.*, **46**, 2153.
[79] KOUCHI, N., UKAI, M., and HATANO, Y., 1997, *J. Phys.* B, **30**, 2319.
[80] BRAGG, S. L., BRAULT, J. W., and SMITH, W. H., 1982, *Astrophys. J.*, **263**, 999.
[81] MOORE, C. E., 1958, *Atomic Energy Levels*, US National Bureau of Standards Circular 467, Vol. I (Washington, DC: US Government Printing Office).
[82] WOLNIEWICZ, L., 1995, *J. chem. Phys.*, **103**, 1792.
[83] BETHE, H. A., and SALPETER, E. E., 1957, *Quantum Mechanics of One and Two Electron Atoms* (Berlin: Springer).
[84] KOUCHI, N., TERAZAWA, N., CHIKAHIRO, Y., UKAI, M., KAMETA, K., HATANO, Y., and TANAKA, K., 1992, *Chem. Phys. Lett.*, **190**, 319.
[85] TERAZAWA, N., KOUCHI, N., UKAI, M., KAMETA, K., HATANO, Y., and ITO, K., 1994, *J. chem. Phys.*, **100**, 7036.
[86] STEPHENS, T. L., and DALGARNO, A., 1974, *Molec. Phys.*, **28**, 1049.
[87] BORRELL, P., GUYON, P. M., and GLASS-MAUJEAN, M., 1977, *J. chem. Phys.*, **66**, 818.